Electronic states of high-T_c cuprate superconductors as studied by the use of the composite-operator approach

M. Sasaki, H. Matsumoto, and M. Tachiki
Institute for Materials Research, Tohoku University, Sendai 980, Japan
(Received 26 December 1991)

The doping dependence of the electronic states in cuprate superconductors is studied by use of the p-d-mixing model. The p-d hopping under strong correlation is treated by introducing electronic excitations associated with Cu-O bonds, which are described by use of composite operators composed of p electrons and neighboring d-electron spin and charge fluctuations. It is shown that changes of electronic states with carrier doping are understood by mixing and decays among those composite electronic excitations. By hole doping, transfer of the density of states to the Fermi level is induced from both the upper Hubbard band and the bottom of the valence band. It is shown that the crossover from a highly correlated electron band to a simple mixing band may be understood by allowing an interchange of energy positions between the upper Hubbard and composite excitation levels. The doping dependence of intrasite charge and spin fluctuations at the Cu site is also discussed. Specially, a prominent intensity transfer to a low-energy region with carrier doping is found to result in the charge fluctuation.

I. INTRODUCTION

All the known high-T_c cuprate superconductors contain CuO_2 planes as common structural elements. The experimental data accumulated so far indicate that the electronic states on the CuO_2 plane are responsible not only for the superconductivity but also for various anomalies in the normal state, such as T-linear dc resistivity, constant continuum of electronic Raman scattering intensity, and so on.[1] The nature of the electronic state on the carrier-doped CuO_2 plane is one of the central issues in the study of high-T_c cuprate superconductors.

The characteristic feature of those cuprate oxides is in fact that one can easily change phases of the system from an insulator to a good metal by a small amount of carrier doping. The superconductivity appears only in a restricted metallic region close to the insulator phase.[2] Extensive experimental studies on the electronic state near the Fermi level (FL) have been performed by photoemission,[3-20] x-ray-absorption spectroscopy[21-25] (XAS), electron-energy-loss spectroscopy[26-28] (EELS), and infrared spectroscopy.[29-36] Those experiments reveal that the parent insulating phase is a charge-transfer (CT) insulator with a gap energy about 1.5-2 eV. Carrier doping on the CuO_2 plane causes great changes in the electronic structure. The rapid accumulation of the state density at the FL with doping is observed in photoemission,[3,13] angle-resolved photoemission,[8,16,20] XAS,[24,25] and EELS,[27] which is not explained by a simple band theory. Upon increasing the state density at the FL, the decrease of the state density at unoccupied lowest-energy levels is indicated in experiments of optical conductivity[29] and XAS.[24,25] For example, the infrared spectral of optical conductivity shows development of the Drude component around the zero-energy range with carrier doping, followed by suppression of CT excitations whose spectral intensity is transferred to a low-energy region. This transfer of the spectral intensity occurs without collapsing the energy-level distances. Further, the angle-resolved photoemission shows the existence of a large Fermi surface,[18] and in this region there are various kinds of evidence suggesting an unconventional normal metallic state,[1] and the superconducting state appears. In a heavily doped region, in turn, the superconductivity disappears and physical properties behave as in an ordinary metal. These kinds of changes with carrier doping are universal for all known hole-doped and electron-doped cuprate superconductors.

The first step to elucidate the mechanism of the high-T_c superconductivity may be to clarify the nature of the electronic state realized in an intermediate region between the CT insulator and the conventional metal. A lot of theoretical models have been proposed to describe the intermediate metallic region. Many of microscopic models are based on the two-dimensional extended Hubbard model, the so-called p-d-mixing model on a square lattice on the CuO_2 plane. Its validity has been discussed in band calculations and from analyses of photoemission and core-level x-ray absorption by cluster calculations.[3,4,37-40] The Hamiltonian is minimally constructed from electrons in Cu $3d_{x^2-y^2}$ and O $2p_\sigma$ (either p_x or p_y) orbitals and includes the mixing interaction t between them as well as the Cu on-site Coulomb repulsion U. Some of models further contain the mixing interaction between O $2p_\sigma$ orbitals and Cu-O intersite Coulomb repulsion V. The p-d-mixing model has been analyzed in the weak-coupling[41-47] and strong-coupling limit,[48-55] or it is further reduced to simpler effective models, such as the one-band Hubbard model,[56-58] t-J model,[59-61] and Kondo-Heisenberg[62-64] model. It has been argued that the electronic state of oxide superconductors is described by a conventional Fermi liquid plus corrections,[65-67] by an exotic state, such as the resonating-valence-bond

(RVB) state,[68] flux state,[69] chiral state in a gauge theory,[70,71] and by a marginal Fermi-liquid state.[72] The nature of the electronic state is still one of the controversial subjects.

Since a system changes its phase drastically from an insulator to a conventional metal by small doping, there arises the question as to which phase the superconducting phase is closer and where one should start an effective theory. To answer this question, one needs to explain doping dependence of the electronic state and to understand causes of the previously mentioned drastic transfer of the state density with carrier doping. In the previous papers, we investigated the doping dependence of the density of states in the highly correlated p-d-mixing model by use of the Green-function method.[51–53] It has been shown that there occurs the transfer of the density of state at the FL inside the charge-transfer gap from both the occupied p band and unoccupied d band, and that a highly correlated electronic state with many-body effects is realized at the FL. Unfortunately, the approximation used in these works breaks down when the carrier density is increased due to nonsufficient inclusion of coherent contributions developed. In this paper, we present a detailed study of the same problem in a slightly different viewpoint, that is, by using a concept of composite electronic excitations associated with Cu-O bonds, and clarify the mechanism of the intensity transfer among several energy levels with carrier doping and describe the crossover from a highly correlated electron state to an ordinary metal.

A detailed formulation of this approach has been presented in the preceding paper.[73] Here we shortly discuss the main idea of the formulation. In the previous papers,[51–53] we started from the electronic states restricted on a single site, and the mutual effects from the neighboring lattices are taken into account as corrections. As the result, we obtain, in addition to the original p and the upper Hubbard bands, the third stable excitation composed of the p-electron and d spin and charge fluctuations. Since we have only two kinds of electron operators, we need to introduce at least one additional composite operator in order to describe third quasistable electronic excitation, i.e., three kinds of quasiparticles are expressed by linear combinations of at least three kinds of operators. The natural candidate in the present problem is a composite operator composed of a p electron and neighboring d spin and charge operators. One may also argue the necessity of composite operators as follows. Through the Pauli principle, the electronic motion is very much restricted by the presence of neighboring electrons; presence of a carrier modifies its surrounding and hopping of the carrier itself is very much affected by such local modification of the electronic state at the neighboring sites. These kinds of effects are hard to include by use of freedoms only restricted at a single site; when one starts from states defined at single site, many corrections are necessary. In other words, in order to express configuration dependence, one needs to introduce composite operators related to several lattice points. Once one realizes the necessity of composite operators to describe a highly correlated electron state, one may reinterpret the role of composite operators to describe the following physical situation. The p and d electronic excitations are not so independent but form electronic excitations on Cu-O bonds as a whole. The energy of the p-electron excitation is, for example, largely modified by the change of charge and spin states of the neighboring Cu ions. A p electron and charge and spin fluctuations on neighboring Cu ions are simultaneously excited; one may imagine an electronic excitation exciting simultaneously its surrounding background. Such excitations are described by composite operators composed of a p electron and d spin and charge fluctuations. We present in this paper results of self-consistent numerical calculations for the electronic density of state by use of the formula obtained in the preceding paper. The doping dependence of both one-particle and two-particle (particle-hole) excitation spectra can be explained qualitatively with clear understanding of level shifts and mixing among composite excitations under consideration, specially it will be shown that the accumulation of the state density at the FL and the intensity transfer among levels are explained in the present scheme. Our present results are qualitatively very similar to those recently obtained by numerical simulations.[74–76]

In the next section, the model is set up and the formulas obtained in the preceding paper are summarized. Explicit formulas used in the numerical calculations are presented in Appendix A. In Sec. III, after the explanation of approximations used in the numerical calculations, results of numerical calculations of the density of states are presented. The mean-field result is shown first to illustrate an approximate energy-level scheme in our approach. Then the results including dynamical corrections are shown. One-particle density of states, local spin, and charge fluctuation spectra are studied in detail by showing their dependence on carrier density, the mixing strength t, and temperature T. It is shown that an enhancement of the density of states at the FL is induced by doping and lowering temperature. The highly correlated states near the FL in the intermediate metallic region are mainly controlled by composite excitations, and the crossover to an ordinary metal is induced through the crossing of the energy levels between shifted composite and upper Hubbard levels. Section IV is devoted for summary and discussions.

II. SUMMARY OF FORMULA

We start from the following p-d-mixing Hamiltonian:

$$H=\sum_i(\varepsilon_d d^\dagger(i)d(i)+Un_\uparrow(i)n_\downarrow(i))+\sum_j\varepsilon_p(p_x^\dagger(i+\tfrac{1}{2}a_x)p_x(i+\tfrac{1}{2}a_x)+p_y^\dagger(i+\tfrac{1}{2}a_y)p_y(i+\tfrac{1}{2}a_y))$$
$$+\sum_i t[d^\dagger(i)\{p_x(i+\tfrac{1}{2}a_x)-p_x(i-\tfrac{1}{2}a_x)-p_y(i+\tfrac{1}{2}a_y)+p_y(i-\tfrac{1}{2}a_y)\}+\text{H.c.}]\,, \tag{2.1}$$

where $d(i)$, $p_x(i+\frac{1}{2}a_x)$, and $p_y(i+\frac{1}{2}a_y)$ are annihilation operators for Cu $3d_{x^2-y^2}$ orbitals at the ith site, O $2p_x$ and $2p_y$ orbitals at the $i+\frac{1}{2}a_x$ and $i+\frac{1}{2}a_y$ sites, respectively. Here the spinor representation is used for electron field operators. In Eq. (2.1), a_x (a_y) indicates the shift of the position in the x (y) direction with a Cu-Cu distance a, $n_\uparrow(i)=d^\dagger_\uparrow(i)d_\uparrow(i)$, $n_\downarrow(i)=d^\dagger_\downarrow(i)d_\downarrow(i)$, and U is an intra-atomic Coulomb repulsion on the Cu ion which is estimated as 7–10 eV. The mixing energy t between the nearest-neighbor p-d electron is about 1 eV. We consider the situation where the d state is Hubbard split and the p level is located between split d levels. The excitation energy for the lower and upper Hubbard levels are ε_d and ε_d+U ($\equiv\varepsilon_\eta$), respectively. The FL is situated between the upper Hubbard level and the p level, which form a CT gap. Since the typical CT gap is about 2 eV and the lower Hubbard band is about 5–8 eV below the p level, the transition to the lower Hubbard band may be neglected to discuss the electronic state near the FL. By taking the limit $U\to\infty$ with keeping ε_η finite, the ionic states of Cu are restricted to Cu^{1+} and Cu^{2+}. In the model (2.1), the Cu^{2+} state is expressed by $n=1$ and the Cu^{1+} state by $n=2$. The transition $n=1\leftrightarrow n=2$ is expressed by the operator $\eta_\sigma(i)$ defined as

$$\eta_\sigma(i)=d_\sigma(i)n_{-\sigma}(i)\ , \tag{2.2}$$

where $n_{-\sigma}(i)=d^\dagger_{-\sigma}(i)d_{-\sigma}(i)$. As for the p electronic excitation, only the following combination of $2p$ orbitals mixes with the $3d$ orbit:

$$p_\gamma(i)=\tfrac{1}{2}[p_x(i+\tfrac{1}{2}a_x)-p_x(i-\tfrac{1}{2}a_x) -p_y(i+\tfrac{1}{2}a_y)+p_y(i-\tfrac{1}{2}a_y)]\ . \tag{2.3}$$

The operator $p_\gamma(i)$ satisfies the commutation relation

$$\{p_\gamma(i),p^\dagger_\gamma(j)\}=\gamma^2(i-j)\ , \tag{2.4}$$

where

$$\gamma^2(i-j)=\delta(i-j)+\gamma_1^2(i-j) \tag{2.5a}$$

with

$$\gamma_1^2(i-j)=-\tfrac{1}{4}[\delta(i-j-a_x)+\delta(i-j+a_x) +\delta(i-j-a_y)+\delta(i-j+a_y)]\ . \tag{2.5b}$$

Their Fourier components are expressed as

$$\gamma^2(\mathbf{k})=\sin^2\frac{k_xa}{2}+\sin^2\frac{k_ya}{2}\ , =1+\gamma_1^2(\mathbf{k}) \tag{2.6a}$$

with

$$\gamma_1^2(\mathbf{k})=-\tfrac{1}{2}(\cos k_xa+\cos k_ya)\ . \tag{2.6b}$$

An orthogonalized set of the bonding p-electron operator $p(i)$ is defined from $p_\gamma(i)$ as

$$p(i)=\left[\frac{\Omega}{(2\pi)^2}\right]^{1/2}\int dk^2p(\mathbf{k})e^{i\mathbf{k}\cdot\mathbf{R}_i}\ , \tag{2.7a}$$

$$p(\mathbf{k})=\left[\frac{1}{\gamma^2(\mathbf{k})}\right]^{1/2}\sum_i p_\gamma(i)e^{-i\mathbf{k}\cdot\mathbf{R}_i} \tag{2.7b}$$

with Ω being the volume of the unit cell, $\mathbf{R}_i$ the lattice point of Cu, and the integration being in the first Brillouin zone. The nonbonding p-electron degree of freedom will be neglected hereafter.

Let us define composite fields composed of the p-electron operator and d spin and charge fluctuations,

$$p_\mu(i)=p_\gamma(i)\delta n_\mu(i)\quad(\mu=0,1,2,3) \tag{2.8}$$

with

$$\delta n_\mu(i)=d^\dagger(i)\sigma_\mu d(i)-\langle d^\dagger(i)\sigma_\mu d(i)\rangle \tag{2.9}$$

and

$$\sigma_\mu=(1,\boldsymbol{\sigma})\ , \tag{2.10}$$

that is, $p_\mu(i)$ represents p electronic excitations in a CuO_2 cluster accompanied by charge ($\mu=0$) and spin ($\mu=1,2,3$) fluctuations of a Cu ion.

Using an abbreviation $p(x)=p(t,i)$, we identify electronic excitations on a Cu-O cluster as $p(x)$, $r(x)$ $[=\sqrt{2/n}\,\eta(x)]$, $p_s(x)=\boldsymbol{\sigma}p_\gamma(x)\mathbf{n}(x)$, and $p_0(x)$ $=p_\gamma(x)\delta n(x)$, where $\mathbf{n}(x)=(n_1(x),n_2(x),n_3(x))$, $\delta n(x)$ $=\delta n_0(x)$, and $n=\langle d^\dagger d\rangle$. Note that the electron fields are in the spinor notation and that $\boldsymbol{\sigma}p_\gamma(x)$, for example, indicates

$$(\boldsymbol{\sigma}p_\gamma(x))_s=\sum_{s'}(\boldsymbol{\sigma})_{ss'}(p_\gamma(x))_{s'}\ .$$

As in the preceding paper, we introduce the notation

$$\psi(x)=\begin{bmatrix}\psi_1(x)\\ \psi_2(x)\\ \psi_3(x)\\ \psi_4(x)\end{bmatrix}=\begin{bmatrix}p(x)\\ r(x)\\ p_s(x)\\ p_0(x)\end{bmatrix}\ , \tag{2.11}$$

and write the equations of motion in the form

$$i\frac{\partial}{\partial t}\psi_l(x)=j_l(x)\ . \tag{2.12}$$

We have

$$j_1(x)=\varepsilon_pp(x)+t_nr_\gamma(x)\ , \tag{2.13a}$$

$$j_2(x)=t_np_\gamma(x)+\varepsilon_\eta r(x)-\frac{t_n}{n}(p_s(x)-p_0(x))\ , \tag{2.13b}$$

$$j_3(x)=\varepsilon_pp_s(x)+t_n(h_s(x)-\psi_s(x)+\varphi_s(x))\ , \tag{2.13c}$$

and

$$j_4(x)=\varepsilon_pp_0(x)+t_n\langle 2-n\rangle r(x) +t_n(h_0(x)-\psi_0(x)+\varphi_0(x))\ , \tag{2.13d}$$

where

$$t_n=2t_0\sqrt{n/2}\ , \tag{2.14}$$

$$h_s(x)=\boldsymbol{\sigma}r_{\gamma_1^2}(x)\mathbf{n}(x),\quad h_0(x)=r_{\gamma_1^2}(x)\delta n(x)\ , \tag{2.15a}$$

$$\psi_s(x)=\boldsymbol{\sigma}p_\gamma(x)\delta\mathbf{n}_+(x),\quad \psi_0(x)=p_\gamma(x)\delta n_+(x)\ , \tag{2.15b}$$

and

$$\varphi_s(x)=\sigma p_\gamma(x)\delta \mathbf{n}_-(x),\quad \varphi_0(x)=p_\gamma(x)\delta n_-(x)\ , \tag{2.15c}$$

with

$$\delta n_{+\mu}(x)=p^\dagger_\gamma(x)\sigma_\mu r(x)-\langle p^\dagger_\gamma(x)\sigma_\mu r(x)\rangle \tag{2.16a}$$

and

$$\delta n_{-\mu}(x)=r^\dagger(x)\sigma_\mu p_\gamma(x)-\langle r^\dagger(x)\sigma_\mu p_\gamma(x)\rangle\ . \tag{2.16b}$$

The abbreviations $r_\gamma(x)$ and $r_{\gamma_1^2}(x)$ mean

$$r_\gamma(x)=\sum_j \gamma(i-j)r(t,j)\ , \tag{2.17a}$$

with

$$\gamma(i-j)=\frac{\Omega}{(2\pi)^2}\int d^2k e^{i\mathbf{k}\cdot(\mathbf{R}_i-\mathbf{R}_j)}[\gamma^2(\mathbf{k})]^{1/2}$$

and

$$r_{\gamma_1^2}(x)=\sum_j \gamma_1^2(i-j)r(t,j)\ . \tag{2.17b}$$

As is seen in Eqs. (2.13a)–(2.13d), $p(x)$, $r(x)$, $p_s(x)$, and $p_0(x)$ mix each other. Time derivatives of $p_s(x)$ and $p_0(x)$ lead us to further complicated fields. Their mixing scheme is summarized in Fig. 1.

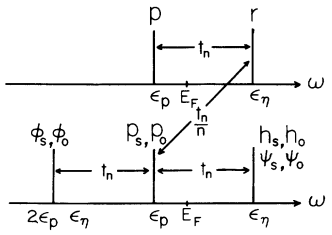

FIG. 1. Mixing scheme among electronic excitations.

The electronic states can be studied by the retarded Green function defined as

$$S_{ln}(x-y)=\langle R\psi_l(x)\psi^\dagger_n(y)\rangle\ , \tag{2.18}$$

where l,n $(=1,2,3,4)$ denote field components, R indicates the retarded time-ordered product, and $\langle\ \rangle$ is the thermal average. Denote the Fourier transform of $S_{ln}(x-y)$ as $S_{ln}(\omega,\mathbf{k})$,

$$S_{ln}(x-y)=\frac{i\Omega}{(2\pi)^3}\int d\omega d^2k\ \exp[-i\omega(t_x-t_y)+i\mathbf{k}\cdot(\mathbf{x}-\mathbf{y})]S_{ln}(\omega,\mathbf{k})\ . \tag{2.19}$$

One has the spectral representation for $S_{ln}(\omega,\mathbf{k})$ as

$$S_{ln}(\omega,\mathbf{k})=\int d\kappa\sigma_{ln}(\kappa,\mathbf{k})\frac{1}{\omega-\kappa+i\delta}\ . \tag{2.20}$$

According to the result of the preceding paper, $S_{ln}(\omega,\mathbf{k})$ is obtained in the form

$$S_{ln}(\omega,\mathbf{k})=\left[I(\mathbf{k})\left[\frac{1}{\omega I(\mathbf{k})-m(\mathbf{k})-\delta m(\omega,\mathbf{k})}\right]I(\mathbf{k})\right]_{ln}\ . \tag{2.21}$$

The one-particle spectral function is obtained by

$$\sigma_{ln}(\omega,\mathbf{k})=-(1/\pi)\mathrm{Im}S_{ln}(\omega,\mathbf{k})\ . \tag{2.22}$$

The matrices $I_{ln}(\mathbf{k})$, $m_{ln}(\mathbf{k})$, and $\delta m_{ln}(\omega,\mathbf{k})$ are shown to satisfy the Hermiticity conditions

$$I(\mathbf{k})=I(\mathbf{k})^\dagger\ , \tag{2.23a}$$

$$m(\mathbf{k})=m(\mathbf{k})^\dagger\ , \tag{2.23b}$$

and

$$\delta m(\omega,\mathbf{k})=\delta m(\omega^*,\mathbf{k})^\dagger\ . \tag{2.23c}$$

and are given in the following.

The normalization matrix $I(\mathbf{k})$ is obtained in the preceding paper as follows:

$$I_{ln}=\begin{bmatrix}1 & 0 & 0 & 0\\ 0 & 1 & 3b & b\\ 0 & 3b & 4a_s+3(\chi_s+\chi_s'\gamma_1^2(\mathbf{k})) & 0\\ 0 & b & 0 & \chi_0+\chi_0'\gamma_1^2(\mathbf{k})\end{bmatrix}, \tag{2.24}$$

where

$$b=\langle p_\gamma r^\dagger\rangle=\langle rp^\dagger_\gamma\rangle\ , \tag{2.25a}$$

$$a_0=\langle p_\gamma p_0^\dagger\rangle,\quad a_s=\langle p_\gamma p_s^\dagger\rangle\ , \tag{2.25b}$$

$$\chi_s=\langle\delta n_i\delta n_i\rangle=\langle 2-n\rangle\ ,\qquad \chi_0=\langle\delta n\delta n\rangle=\langle 2-n\rangle\langle n-1\rangle \tag{2.25c}$$

and

$$\chi_s'=-\langle\gamma_1^2\delta n_i\delta n_i\rangle,\quad \chi_0'=-\langle\gamma_1^2\delta n\delta n\rangle\ . \tag{2.25d}$$

Since there is the Hermiticity requirement for $m(\mathbf{k})$, it is enough to evaluate the upper half components of the matrix $m(\mathbf{k})$. The mean field $m(\mathbf{k})$ is obtained as

$$m_{11}=\varepsilon_p\ , \tag{2.26a}$$

$$m_{12}=t_n\gamma(\mathbf{k})\ , \tag{2.26b}$$

$$m_{13}=3t_nb\gamma(\mathbf{k})\ , \tag{2.26c}$$

$$m_{14}=t_nb\gamma(\mathbf{k})\ , \tag{2.26d}$$

$$m_{22}=\varepsilon_\eta-2b\frac{t_n}{n}\ , \tag{2.27a}$$

$$m_{23}=3\varepsilon_\eta b-\frac{t_n}{n}(3(\chi_s+\chi_s'\gamma_1^2(\mathbf{k}))+4a_s)\ , \tag{2.27b}$$

$$m_{24}=\varepsilon_\eta b+\frac{t_n}{n}(\chi_0+\chi_0'\gamma_1^2(\mathbf{k}))\ , \tag{2.27c}$$

$$m_{33}=\varepsilon_p(3(\chi_s+\chi_s'\gamma_1^2(\mathbf{k}))+4a_s) +t_n(4b_s'+6b(a-1)-\tfrac{3}{2}(\chi'_{+0s}-\chi'_{-0s})\gamma_1^2(\mathbf{k}))\ , \tag{2.28a}$$

$$m_{34}=t_n(-6ab+(2-n)3b-\tfrac{3}{2}(\chi'_{+0s}+\chi'_{0-\rho})\gamma_1^2(\mathbf{k}))\ , \tag{2.28b}$$

and

$$m_{44}=\varepsilon_p(\chi_0+\chi_0'\gamma_1^2(\mathbf{k})) +t_n[\chi_s b+b(2a-n)-\tfrac{1}{2}(3\chi'_{0+\rho}+\chi'_{0=\rho})\gamma_1^2(\mathbf{k})]\ , \tag{2.29}$$

where

$$b_s'=-\langle r_{\gamma_1^2}p_s^\dagger\rangle=-\langle p_s r_{\gamma_1^2}^\dagger\rangle\ , \tag{2.30a}$$

$$\chi'_{+0\mu}=-\langle\gamma_1^2\delta n_{+\mu}\delta n_\mu\rangle\ , \tag{2.30b}$$

and

$$\chi'_{-0\mu}=-\langle\gamma_1^2\delta n_{-\mu}\delta n_\mu\rangle\ . \tag{2.30c}$$

The dynamical correction $\delta m(\omega,\mathbf{k})$ is obtained from the decay processes induced by $h_{s,0}$, $\psi_{s,0}$, and $\varphi_{s,0}$ defined in Eq. (2.15). Since composite excitations are expected to be of local nature, we neglect $\mathbf{k}$ dependence of $\delta m(\omega,\mathbf{k})$ in this paper, and effects of decay processes are evaluated for localized states in a Cu-O cluster. We approximate $\delta m(\omega,\mathbf{k})$ by one loops composed of fermion and fluctuation propagators. By neglecting the interference among different decay processes, we evaluate $\delta m(\omega,\mathbf{k})$ by

$$\delta m_{33}(x-y)\approx t_n\{G_{h_sh_s^\dagger}(x-y)+G_{\psi_s\psi_s^\dagger}(x-y) +G_{\varphi_s\varphi_s^\dagger}(x-y)\}\ , \tag{2.31a}$$

$$\delta m_{34}(x-y)\approx t_n\{G_{h_sh_0^\dagger}(x-y)+G_{\psi_s\psi_0^\dagger}(x-y) +G_{\varphi_s\varphi_0^\dagger}(x-y)\}\ , \tag{2.31b}$$

and

$$\delta m_{44}(x-y)\approx t_n\{G_{h_0h_0^\dagger}(x-y)+G_{\psi_0\psi_0^\dagger}(x-y) +G_{\varphi_0\varphi_0^\dagger}(x-y)\}\ , \tag{2.31c}$$

where the Green functions G are defined as

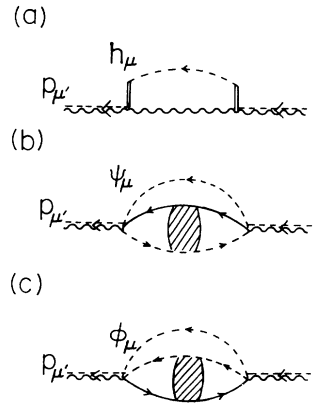

FIG. 2. Loop diagrams for dynamical corrections. Each line indicates the propagation of the following mode: the dotted line for the p electron, the solid line for the d electron, the dotted-wavy line for composite electrons, and the wavy line for spin and charge fluctuations of the d electron. The double solid line indicates γ_1^2 representing the nearest-neighbor site. The shaded bubble indicates the fluctuations formed by $\delta n_{\pm\mu}$.

$$G_{h_sh_s^\dagger}(x-y)=\langle Rh_s(x)h_s^\dagger(y)\rangle_{\text{irr}}$$

and so on, with the suffix "irr" indicating an irreducible part of the ψ line. These functions correspond to one-loop diagrams in Fig. 2 of the fermion ψ line and spin and charge fluctuation lines. Let us define spectral functions of spin and charge fluctuations $\rho_{lk}^\mu(\omega,\mathbf{k})$ given by the Fourier transform of $\rho_{lk}^\mu(x-y)$ with

$$\rho_{lk}^\mu(x-y)=\langle[\delta n_{l_\mu}(x),\delta n_{k_\mu}^\dagger(y)]\rangle\ , \tag{2.32}$$

where $\mu=0$ (for charge), $\mu=1,2,3$ (for spin), and l and k indicate components of fluctuations $0,\pm$ as

$$\delta n_{l_\mu}(x)=\begin{bmatrix}\delta n_\mu(x)\\ \delta n_{+\mu}(x)\\ \delta n_{-\mu}(x)\end{bmatrix}\ , \tag{2.33}$$

where $\delta n_{\pm\mu}(x)$ is given in Eq. (2.16). The spectral function of the lowest bubble diagrams shown in Fig. 3(a) is

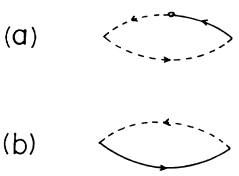

FIG. 3. Lowest bubble diagrams for fluctuations. (a) $p_\gamma^\dagger\sigma_\mu p_\gamma$-$(\delta n_{+\mu})^\dagger$ fluctuation; (b) $(\delta n_{-\mu})$-$(\delta n_{-\mu})^\dagger$ fluctuation.

given by

$$b_{p_+}(\omega,\mathbf{k})=\int d\nu[f_F(\nu)-f_F(\nu+\omega)] \times\frac{\Omega}{(2\pi)^2}\int d^2q\,tr[\sigma_\mu\sigma_{p_\gamma r}{}^\dagger(\nu+\omega,\mathbf{q}+\mathbf{k}) \times\sigma_\mu\sigma_{p_\gamma p_\gamma^\dagger}{}^\dagger(\nu,\mathbf{q})] \tag{2.34a}$$

and that of Fig. 3(b) is given by

$$b_{--}(\omega,\mathbf{k})=\int d\nu[f_F(\nu)-f_F(\nu+\omega)] \times\frac{\Omega}{(2\pi)^2}\int d^2q\,tr[\sigma_\mu\sigma_{p_\gamma p_\gamma^\dagger}{}^\dagger(\nu+\omega,\mathbf{q}+\mathbf{k}) \times\sigma_\mu\sigma_{rr}{}^\dagger(\nu,\mathbf{q})] , \tag{2.34b}$$

where $f_F(\omega)$ is the Fermi distribution function. Then the spectral functions $g(\omega,\mathbf{k})$ of $G(\omega,\mathbf{k})$ in Eq. (2.31) are evaluated as

$$g_{h_s h_s^\dagger}(\omega,\mathbf{k})=\int d\nu\theta(\omega,\nu)\frac{\Omega}{(2\pi)^2}\int d^2q\,3\rho^s_{00}(\omega-\nu,\mathbf{k}-\mathbf{q})\gamma_1^2(\mathbf{q})\sigma_{rr}{}^\dagger(\nu,\mathbf{q})\gamma_1^2(\mathbf{q}) , \tag{2.35a}$$

$$g_{h_0 h_0^\dagger}(\omega,\mathbf{k})=\int d\nu\theta(\omega,\nu)\frac{\Omega}{(2\pi)^2}\int d^2q\,\rho^0_{00}(\omega-\nu,\mathbf{k}-\mathbf{q})\gamma_1^2(\mathbf{q})\sigma_{rr}{}^\dagger(\nu,\mathbf{q})\gamma_1^2(\mathbf{q}) , \tag{2.35b}$$

$$g_{\psi_s\psi_s^\dagger}(\omega,\mathbf{k})=\int d\nu\theta(\omega,\nu)\frac{\Omega}{(2\pi)^2}\int d^2q\{3\rho^s_{++}(\omega-\nu,\mathbf{k}-\mathbf{q})\sigma_{p_\gamma p_\gamma^\dagger}{}^\dagger(\nu,\mathbf{q})+\tfrac{3}{2}b_{p_+}(\omega-\nu,\mathbf{k}-\mathbf{q})\sigma_{rp_\gamma^\dagger}{}^\dagger(\nu,\mathbf{q})\} , \tag{2.36a}$$

$$g_{\psi_s\psi_0^\dagger}(\omega,\mathbf{k})=\int d\nu\theta(\omega,\nu)\frac{\Omega}{(2\pi)^2}\int d^2q(-\tfrac{3}{2})b_{p_+}(\omega-\nu,\mathbf{k}-\mathbf{q})\sigma_{rp_\gamma^\dagger}{}^\dagger(\nu,\mathbf{q}) , \tag{2.36b}$$

$$g_{\psi_0\psi_0^\dagger}(\omega,\mathbf{k})=\int d\nu\theta(\omega,\nu)\frac{\Omega}{(2\pi)^2}\int d^2q\{\rho^0_{++}(\omega-\nu,\mathbf{k}-\mathbf{q})\gamma^2(\mathbf{q})\sigma_{pp}{}^\dagger(\nu,\mathbf{q})-\tfrac{1}{2}b_{p_+}(\omega-\nu,\mathbf{k}-\mathbf{q})\sigma_{rp_\gamma^\dagger}{}^\dagger\} , \tag{2.36c}$$

$$g_{\varphi_s\varphi_s^\dagger}(\omega,\mathbf{k})=9g_{\varphi_0\varphi_0^\dagger}(\omega,\mathbf{k}) , \tag{2.37a}$$

$$g_{\varphi_s\varphi_0^\dagger}(\omega,\mathbf{k})=-3g_{\varphi_0\varphi_0^\dagger}(\omega,\mathbf{k}) , \tag{2.37b}$$

and

$$g_{\varphi_0\varphi_0^\dagger}(\omega,\mathbf{k})=\int d\nu\theta(\omega,\nu)\frac{\Omega}{(2\pi)^2}\int d^2q\tfrac{1}{4}\{\rho^0_{--}(\omega-\nu,\mathbf{k}-\mathbf{q})+3\rho^s_{--}(\omega-\nu,\mathbf{k}-\mathbf{q})-2b_{--}(\omega-\nu,\mathbf{k}-\mathbf{q})\}\sigma_{p_\gamma p_\gamma^\dagger}{}^\dagger(\nu,\mathbf{q}) , \tag{2.37c}$$

where

$$\theta(\omega,\nu)=[1+f_B(\omega-\nu)]f_F(-\nu)+f_B(\omega-\nu)f_F(\nu) \tag{2.38}$$

and $\rho^s_{lk}(\omega,\mathbf{k})$ is $\rho^i_{lk}(\omega,\mathbf{k})$ $(i=1,2,3)$ and $f_B(\omega)$ is the Bose distribution function.

The relevant spin and charge fluctuations to the dynamical correction $\delta m(\omega,\mathbf{k})$ of one-particle states are described by the field operators $\delta n_{l_\mu}(x)$ defined by Eq. (2.33). In order to calculate the energy spectrum of intrasite spin and charge fluctuations, we use the relaxation function. In the preceding paper, the spectral functions of intrasite fluctuations are expressed in the form

$$\rho^\mu_{lk}(\omega)=R^\mu_{lk}(\omega)+\alpha^\mu_l R^\mu_{0k}(\omega)+R^\mu_{l0}(\omega)\alpha^\mu_k+\alpha^\mu_l R^\mu_{00}(\omega)\alpha^\mu_k \tag{2.39}$$

with $R^\mu_{lk}(\omega)$ being given by

$$R^\mu_{lk}(\omega)=-\frac{\omega}{\pi}\mathrm{Im}\left[F^\mu\frac{1}{\omega F^\mu-M^\mu_0-\delta M^\mu(\omega)}F^\mu\right] , \tag{2.40}$$

where α^μ_l, F^μ, M^μ_0, and $\delta M^\mu(\omega)$ have the forms

$$\alpha^\mu_l=(0,\alpha_0\delta_{\mu 0}+\alpha_s\delta_{\mu i},\alpha_0\delta_{\mu 0}+\alpha_s\delta_{\mu i}) , \tag{2.41}$$

$$F^\mu=\begin{bmatrix} F^\mu_{00} & 0 & 0 \\ 0 & F^\mu_{++} & F^\mu_{+-} \\ 0 & F^{\mu *}_{+-} & F^\mu_{++} \end{bmatrix} , \tag{2.42}$$

$$M_0^\mu = \begin{pmatrix} 0 & (M_0^\mu)_{0+} & -(M_0^\mu)^*_{0+} \\ (M_0^\mu)^*_{0+} & (M_0^\mu)_{++} & 0 \\ -(M_0^\mu)_{0+} & 0 & -(M_0^\mu)_{++} \end{pmatrix}, \tag{2.43}$$

and

$$\delta M^\mu(\omega) = \begin{pmatrix} 0 & 0 & 0 \\ 0 & \delta M^\mu_{++}(\omega+i\delta) & \delta M^\mu_{+-}(\omega+i\delta) \\ 0 & \delta M^{\mu *}_{+-}(\omega+i\delta) & \delta M^\mu_{++}(-\omega+i\delta) \end{pmatrix}. \tag{2.44}$$

The values of α_l^μ, F^μ, and $(M_0^\mu)_{lk}$ are self-consistently determined from

$$X_{lk}^\mu = \int d\omega \left[-\frac{1}{\pi} \right] \mathrm{Im} \left[\frac{1}{\omega - \Sigma^\mu(\omega)} F^\mu \right]_{lk} \omega(1+f_B(\omega)) \tag{2.45}$$

and

$$Y_{lk}^\mu = \int d\omega \left[-\frac{1}{\pi} \right] \mathrm{Im} \left[\Sigma^\mu(\omega) \frac{1}{\omega - \Sigma^\mu(\omega)} F^\mu \right]_{lk} \omega(1+f_B(\omega)) , \tag{2.46}$$

with

$$\Sigma^\mu(\omega) = (M_0^\mu + \delta M^\mu(\omega)) F^{\mu -1} , \tag{2.47}$$

$$X_{lk}^\mu = x_{lk}^\mu - \alpha_l^\mu x_{0k}^\mu - x_{l0}^\mu \alpha_k^\mu + \alpha_l^\mu x_{00}^\mu \alpha_k^\mu , \tag{2.48a}$$

and

$$Y_{lk}^\mu = y_{lk}^\mu - \alpha_l^\mu y_{0k}^\mu - y_{l0}^\mu \alpha_k^\mu + \alpha_l^\mu y_{00}^\mu \alpha_k^\mu . \tag{2.48b}$$

The explicit forms of x_{lk}^μ and y_{lk}^μ are given as

$$x_{lk}^0 = \begin{pmatrix} (n-1)(2-n) & -2b(2-n) & -2b(1-n) \\ -2b(2-n) & 2\left\{ \frac{2-n}{n}(1-a) + \frac{1}{n}(a_0+a_s) - 2b^2 \right\} & -4b^2 \\ -2b(1-n) & -4b^2 & 4\left\{ \frac{n-1}{n}a + \frac{1}{n}a_0 - b^2 \right\} \end{pmatrix} \tag{2.49a}$$

and

$$x_{lk}^i = \begin{pmatrix} 2-n & 0 & 2b \\ 0 & 2\left\{ \frac{2-n}{n}(1-a) + \frac{1}{n}(a_0-a_s) \right\} & 0 \\ 2b & 0 & 4\left\{ \frac{n-1}{n}a + \frac{1}{n}a_0 \right\} \end{pmatrix}, \tag{2.49b}$$

where $a = \langle p_\gamma p_\gamma^\dagger \rangle$, $b = \langle p_\gamma r^\dagger \rangle$, $a_0 = \langle p_\gamma p_0^\dagger \rangle$, and $a_s = \langle p_\gamma p_s^\dagger \rangle$, and

$$y_{lk}^\mu = \begin{pmatrix} t_n(x^\mu_{-k} - x^\mu_{+k}) \\ (\varepsilon_\eta - \varepsilon_p) x^\mu_{+k} + c_\mu x^\mu_{0k} \\ -(\varepsilon_\eta - \varepsilon_p) x^\mu_{-k} - c_\mu x^\mu_{0k} \end{pmatrix} + \delta y_{lk}^\mu , \tag{2.50}$$

with

$$\delta y^\mu_{++} = \frac{t_n}{n} \{ 4(1-a)b - 2(2-n)b' - \delta_{\mu 0}(b_0' + b_s') - \delta_{\mu i}(b_0' - \tfrac{1}{3} b_s') \} , \tag{2.51a}$$

$$\delta y^\mu_{+-} = t_n \left\{ -2ab + ab \left[-\frac{4-n}{n}\delta_{\mu 0} + \delta_{\mu i} \right] - 2b a_r' \right\} , \tag{2.51b}$$

and

$$\delta y^{\mu}_{--}=-\frac{t_n}{n}\{8ab+4(n-1)b'-2b'_0\}\ , \tag{2.51c}$$

where $a'_r=-\langle r_{\gamma_1^2}r^{\dagger}\rangle$, $b=\langle p_{\gamma}r^{\dagger}\rangle$, $b'=-\langle p_{\gamma}r^{\dagger}_{\gamma_1^2}\rangle$, $b'_0=\langle p_0 r^{\dagger}_{\gamma_1^2}\rangle$, and $b'_s=\langle p_s r^{\dagger}_{\gamma_1^2}\rangle$.

The dynamical correction $\delta M^{\mu}(\omega)_{lk}$ is estimated from particle-hole pair excitations induced by the source

$$\delta j_{+\mu}(x)=t_n\left[p^{\dagger}_{\gamma}(x)\sigma_{\mu}p_{\gamma}(x)-\frac{1}{n}p^{\dagger}_{\gamma}(x)\sigma_{\mu}\sigma^{\lambda}p_{\gamma}(x)\delta n_{\lambda}(x)-r^{\dagger}_{\gamma_1^2}(x)\sigma_{\mu}r(x)\right] \tag{2.52a}$$

and

$$\delta j_{-\mu}(x)=t_n\left[p^{\dagger}_{\gamma}(x)\sigma_{\mu}p_{\gamma}(x)-\frac{1}{n}p^{\dagger}_{\gamma}(x)\sigma^{\lambda}\sigma_{\mu}p_{\gamma}(x)\delta n_{\lambda}(x)-r^{\dagger}(x)\sigma_{\mu}r_{\gamma_1^2}(x)\right]\ . \tag{2.52b}$$

Let us denote the one-loop response function of $\delta j_{\pm}(x)$ as $J_{++}(\omega)$ and $J_{+-}(\omega)$,

$$\langle R\,\delta j_{+\mu}(t)\delta j^{\dagger}_{+\mu}(t')\rangle=\frac{i}{2\pi}\int d\omega e^{-i\omega(t-t')}J^{\mu}_{++}(\omega) \tag{2.53a}$$

and

$$\langle R\,\delta j_{+\mu}(t)\delta j^{\dagger}_{-\mu}(t')\rangle=\frac{i}{2\pi}\int d\omega e^{-i\omega(t-t')}J^{\mu}_{--}(\omega)\ . \tag{2.53b}$$

We have

$$\delta M^{\mu}_{+\pm}=\pm\int d\kappa\left[-\frac{1}{\pi\kappa}\mathrm{Im}J^{\mu}_{+\pm}(\kappa)\right]\frac{1}{\omega-\kappa+i\delta}\ . \tag{2.54}$$

The detailed expressions for $\delta M^{\mu}(\omega)$ are given in Appendix A. Once the one-particle propagator of ψ is determined, X^{μ}, Y^{μ}, and $\delta M^{\mu}(\omega)$ are calculated first by Eqs. (2.48), (2.49), and the formula in Appendix A, and then F^{μ} and M^{μ}_0 can be determined to satisfy Eqs. (2.45) and (2.46).

Finally, it is worth noticing that the spectral functions $\rho^{\mu}_{lk}(\omega)$ are related from the following relations which are easily obtained by the fact that $\delta n_{+\mu}$ and $\delta n_{-\mu}$ are Hermitian conjugate,

$$\rho^{\mu}_{0-}(\omega)=-\rho^{\mu}_{0+}(-\omega)\ , \tag{2.55a}$$

$$\rho^{\mu}_{-0}(\omega)=-\rho^{\mu}_{0+}(-\omega)\ , \tag{2.55b}$$

$$\rho^{\mu}_{--}(\omega)=-\rho^{\mu}_{++}(-\omega)\ , \tag{2.55c}$$

$$\rho^{\mu}_{+0}(\omega)=-\rho^{\mu}_{0+}(-\omega)\ , \tag{2.55d}$$

and

$$\rho^{\mu}_{-+}(\omega)=\rho^{\mu}_{+-}(\omega)\ . \tag{2.55e}$$

Finally, we comment on our approximation scheme in comparison with the Hubbard approximation. In our scheme, the expression of the propagator in Eq. (2.21) is quite general and the approximation comes in the evaluation of $I(\mathbf{k})$, $m(\mathbf{k})$, and $\delta m(\omega,\mathbf{k})$. We may say that the present interest is in the propagation property of ψ_n and that contributions from other possible modes are amalgamated in $I(\mathbf{k})$, $m(\mathbf{k})$, and $\delta m(\omega,\mathbf{k})$. In the Hubbard approximation, the self-energy

$$\Sigma(\omega,\mathbf{k})=(m(\mathbf{k})+\delta m(\omega,\mathbf{k}))I(\mathbf{k})^{-1}$$

is directly evaluated by use of the equation of motion (2.12) in combination with the point splitting method and the introduction of certain decomposition rules such as the random-phase approximation. As was mentioned in the preceding paper, due to the nonidentity property of $I(\mathbf{k})$, it is rather difficult to find the condition for $\Sigma(\omega,\mathbf{k})$ to satisfy the necessary requirements for the total propagator, specially when one uses the corrected full propagators for the evaluation of $\Sigma(\omega,\mathbf{k})$. We approximately evaluate $\delta m(\omega,\mathbf{k})$ by the one-loop continuum composed of full propagators of quasistable electronic excitations and fluctuations, following the spirit of loop expansions in terms of renormalized quasistable excitations. Although $\delta m(\omega,\mathbf{k})$ is one loop, the full propagators contain infinite order of the repetition of loops through the mixing scheme induced by $m(\mathbf{k})$ and $I(\mathbf{k})$.

III. NUMERICAL CALCULATION AND RESULTS

In our calculation, the given parameters are bare excitation level ε_p (for the O $2p$ state), ε_η (for the upper Hubbard level of the Cu $3d$ state), p-d-mixing interaction t, and temperature T. Small but finite damping constants γ and γ_ρ are introduced for numerical calculation. We replace $\varepsilon_p,\varepsilon_\eta$ by $\varepsilon_p-i\gamma$, $\varepsilon_\eta-i\gamma$, respectively, in $m(\mathbf{k})$ of Eqs. (2.26a)–(2.29), and ωF^{μ} by $(\omega+i\gamma_\rho)F^{\mu}$ in Eq. (2.40). The origin of energy is taken at the chemical potential and the d- and p-electron numbers n and n_p, respectively, are determined from[51–53]

$$n_p=2\int d\omega\frac{\Omega}{(2\pi)^2}\int d^2q\,\sigma_{pp^{\dagger}}(\omega,\mathbf{k})f_F(\omega)\ , \tag{3.1a}$$

$$\frac{2}{n}-1=2\int d\omega\frac{\Omega}{(2\pi)^2}\int d^2q\,\sigma_{rr^{\dagger}}(\omega,\mathbf{k})(1-f_F(\omega)) \tag{3.1b}$$

under given parameters ε_p, ε_η, t, T, γ, and γ_ρ.

The equations listed in the preceding section form a set of self-consistent equations. We apply a simple iteration technique to solve those self-consistent integral equations. We express p- and d-electron Green functions $S_{pp^{\dagger}}(\omega,\mathbf{k})$ and $S_{\eta\eta^{\dagger}}(\omega,\mathbf{k})$ in the following forms by introducing the one-p-electron irreducible part $\tilde{S}_{\eta\eta^{\dagger}}(\omega,\mathbf{k})$ of $S_{\eta\eta^{\dagger}}(\omega,\mathbf{k})$:

$$S_{pp^{\dagger}}(\omega,\mathbf{k})=\frac{1}{\omega-\varepsilon_p-t^2(\mathbf{k})S_{\eta\eta^{\dagger}}(\omega,\mathbf{k})}\ , \tag{3.2a}$$

$$S_{\eta\eta^{\dagger}}(\omega,\mathbf{k})=\frac{(\omega-\varepsilon_p)\tilde{S}_{\eta\eta^{\dagger}}(\omega,\mathbf{k})}{\omega-\varepsilon_p-t^2(\mathbf{k})S_{\eta\eta^{\dagger}}(\omega,\mathbf{k})}\ , \tag{3.2b}$$

where $t^2(\mathbf{k})=4t^2\gamma^2(\mathbf{k})$ and $S_{\eta\eta^{\dagger}}(\omega,\mathbf{k})=(n/2)S_{rr^{\dagger}}(\omega,\mathbf{k})$.

By introducing $\Sigma_\eta(\omega,\mathbf{k})$ further, we express the one-p-electron irreducible part as

$$\tilde{S}_{\eta\eta^\dagger}(\omega,\mathbf{k})=\frac{n/2}{\omega-\tilde{\varepsilon}_\eta-\Sigma_\eta(\omega,\mathbf{k})} . \tag{3.3}$$

The expression of $\Sigma_\eta(\omega,\mathbf{k})$ is given in Appendix B. Those expressions are convenient for physical interpretation in the later discussion.

Since $\mathbf{k}$ dependence appears only through $\gamma_1^2(\mathbf{k})$ [here note that $\gamma^2(\mathbf{k})=1+\gamma_1^2(\mathbf{k})$], $\sigma_{\psi_n\psi_n^\dagger}(\omega,\mathbf{k})$ is given in the form $\sigma_{\psi_n\psi_n^\dagger}(\omega,\gamma_1^2(\mathbf{k}))$, and $\mathbf{k}$ integration can be performed to get the one-particle density of state as

$$\sigma_{\psi_n\psi_n^\dagger}(\omega)=\frac{\Omega}{(2\pi)^2}\int d^2k\,\sigma_{\psi_n\psi_n^\dagger}(\omega,\gamma_1^2(\mathbf{k})) \tag{3.4a}$$

$$=\int dx W(x)\sigma_{\psi_n\psi_n^\dagger}(\omega,x) , \tag{3.4b}$$

where the function $W(x)$ is defined as

$$W(x)=\frac{\Omega}{(2\pi)^2}\int d^2k\,\delta(x-\gamma_1^2(\mathbf{k})) . \tag{3.5}$$

In the present paper, the $\mathbf{k}$ dependence of $I(\mathbf{k})$ in Eqs. (2.24), $m_{23}(\mathbf{k})$, $m_{24}(\mathbf{k})$, $m_{33}(\mathbf{k})$, $m_{34}(\mathbf{k})$, $m_{44}(\mathbf{k})$ in Eqs. (2.27b)–(2.29) and $\delta m(\omega,\mathbf{k})$ will be neglected, since the composite operators are primarily of local nature.

Since the function $W(x)$ given in Eq. (3.5) has the van Hove singularity at $x=0$ which makes time for convergency longer, we replace $W(x)$ in Eq. (3.5) by

$$W(x)=\tfrac{1}{2}\Theta(x+1)\Theta(1-x) , \tag{3.6}$$

which is equivalent to the approximation

$$\gamma_1^2(\mathbf{k})\sim\frac{\Omega}{2\pi}k^2-\frac{2\pi}{\Omega} , \tag{3.7}$$

or to the approximation used in the Ref. 53. The shapes of the density of states $\sigma_{\psi_n\psi_n^\dagger}(\omega)$ depend on which form of $W(x)$ is used. However, the analysis shows that the essential result at the FL in the present p-d-mixing model is insensitive to the choice of $W(x)$.

First, we show the results of mean-field approximation where the dynamical correction $\delta m(\omega,\mathbf{k})$ is neglected. The renormalized energy levels of modes p, η, p_s, and p_0 are self-consistently determined, and therefore the lattice effect is taken into account in the static approximation. In Fig. 4 we present the density of states of p [$2\sigma_{pp^\dagger}(\omega)$, where the factor 2 is for spin up and down, fine solid lines] and d [$\sigma_{\eta\eta^\dagger}(\omega)$, bold solid lines] electrons with hole doping. We choose parameters as $t=0.5$ eV, Δ_0 ($\equiv\varepsilon_\eta-\varepsilon_p$)$=1.2$ eV, $\gamma=0.05$, and temperature $T=0.05$ eV. By fixing Δ_0, we change ε_p as (a) -1.1 eV, (b) -0.7 eV, and (c) -0.38 eV whose positions are indicated by the dashed lines in Fig. 4. The obtained constants are summarized in Table I, where n_d is n obtained from (3.1b), the hole density n_h defined as the reduction of total electron number with respect to case (a).

In the mean-field approximation, a four-peak structure is expected, since there are four levels corresponding to p, η, p_s, and p_0. In fact, the calculated density of states is composed of three main peaks and one satellite peak. The first main peak at higher energy is the upper Hubbard band which is largely of Cu d character. The other two main peaks are mainly of O p character. Since $t^2(\mathbf{k})=0$ at $\mathbf{k}=\mathbf{0}$ in the present model, the d electronic state never mixes with the p electronic state with $\mathbf{k}=\mathbf{0}$ so that the d-electron density of states vanishes at $\omega=\varepsilon_p$. The bare p band is strongly renormalized and split into two peaks around $\omega=\varepsilon_p$.

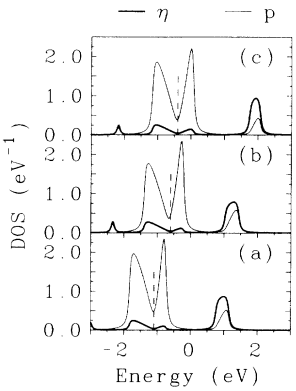

FIG. 4. Mean-field result of the density of states for p (fine solid line) and d (bold solid line) electrons. Parameters are $t=0.5$ eV, $\Delta_0=1.2$ eV and ε_p is changed as (a) -1.1 eV, (b) -0.7 eV, and (c) -0.38 eV, which is indicated by the dotted line.

In Fig. 5 we show the density of states of the composite states, $\frac{1}{9}\sigma_{p_sp_s^\dagger}(\omega)$ (solid lines) and $\sigma_{p_0p_0^\dagger}(\omega)$ (dashed lines). The state near the FL is dominated by the component of p_s, while the state corresponding to the upper Hubbard band by the component of p_0. The satellite peak has the mixture of p_0 and p_s. The reason for this can be easily understood by considering Eqs. (2.13c) and (2.13d). The operator p_0 mixes with r directly, while p_s does not. This is due to the local constraints of $r\delta n_0=2r$ and $r\mathbf{n}=\mathbf{0}$. Around ε_p, p_0 mixes with p through δn_0, whose contribution is small, while p_s mixes with p by changing spin states, which is the main mixing. It is easily shown that the renormalized excitation level of p_s is around $\varepsilon_p+t_n^2/\Delta_0$, that is, the splitting of the bare p band is

TABLE I. Calculated physical constants for given ε_p (without dynamical corrections).

	(a)	(b)	(c)
ε_p	-1.1 eV	-0.6 eV	-0.4 eV
n_p	1.794	1.731	1.563
n_d	1.200	1.241	1.223
n_h	0.000	0.023	0.210
a	0.128	0.165	0.275
b	0.241	0.253	0.264
a_0	0.068	0.079	0.085
a_s	-0.015	0.000	0.263

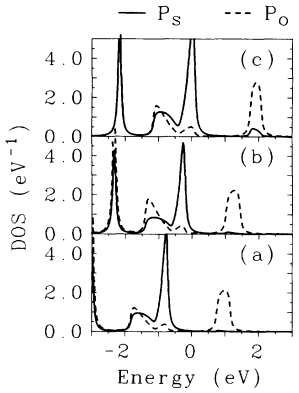

FIG. 5. Mean-field result of $\frac{1}{9}\sigma_{p_s p_s^\dagger}(\omega)$ (solid line) and $\sigma_{p_0 p_0^\dagger}(\omega)$ (dashed line). Parameters are the same as in Fig. 4.

mainly due to the mixing with p_s.

The change with doping is, roughly speaking, rigid-band-like in this mean-field approximation, although the band near the FL becomes wider and the upper Hubbard band becomes slightly narrower in bandwidth. The values of b, a_0, and a_s are all increased by doping.

Next, we present the results with dynamical correction. In Fig. 6 we show the density of states of the p (fine solid lines) and d (bold solid lines) electron with increasing hole doping. Given parameters are same as in Fig. 4, except for $\gamma_p=0.05$ eV. The obtained constants are summarized in Table II. In contrast to the results in Fig. 4, the electronic structure is sensitive to doping. In an insulating case (a), there are two bands, one is the upper Hubbard band, another is the valence which is mainly p character and shows the precursor of splitting around $\omega=\varepsilon_p$. As doping proceeds, a state develops at the FL forming three-peak structure. The upper Hubbard band moves to higher energy and its intensity is decreased especially in the p-electron component mixed in the upper level. The weight at the bottom of p band also decreases. The peak structure of Fig. 6 is similar to those obtained in numerical simulations.[74–76]

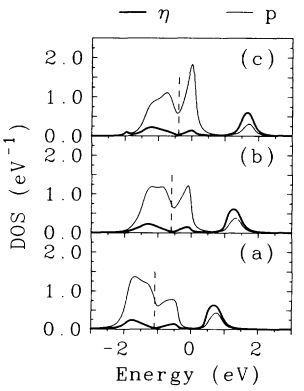

FIG. 6. Density of states for p (fine solid line) and d (bold solid line) electrons. Parameters are $t=0.5$ eV, $\Delta_0=1.2$ eV and ε_p is changed as (a) -1.1 eV, (b) -0.6 eV, and (c) -0.4 eV, which is indicated by the dotted line.

TABLE II. Calculated physical constants for given ε_p (with dynamical corrections).

	(a)	(b)	(c)
ε_p	-1.1 eV	-0.6 eV	-0.4 eV
n_p	1.724	1.647	1.473
n_d	1.277	1.268	1.272
n_h	0.000	0.086	0.256
a	0.166	0.215	0.321
b	0.241	0.257	0.280
a_0	0.076	0.080	0.093
a_s	-0.011	0.073	0.269
c_s	0.057	0.113	0.231
c_t	0.192	0.194	0.155

In Fig. 7 we show the spectral densities $\sigma_{pp^\dagger}(\omega,\mathbf{k})$ and $\sigma_{\eta\eta^\dagger}(\omega,\mathbf{k})$ for the metallic case of Fig. 5(c). A quasiparticle band crosses the FL and it has a large Fermi surface. The precursor of this band can be seen, in the insulator phase, as a damping mode on the top of the valence band, as is shown in Fig. 8 [which corresponds to the case of Fig. 5(a)].

In Fig. 9 the densities of states of p_s [$\frac{1}{9}\sigma_{p_s p_s^\dagger}(\omega)$, solid lines] and p_0 [$\sigma_{p_0 p_0^\dagger}(\omega)$, dashed lines] are presented. Drastic change by doping occurs in the p_s component. In an insulating case (a), p_s has a peak around $\omega\sim-1.6$ eV, but this state has damping nature because it overlaps with continua from h_μ, ψ_μ, and φ_μ, as is shown in Fig. 10. By doping, this p_s state shifts its weight rapidly at the FL and increases its intensity, forming a sharp narrow band. From these results, we may say that the state near the FL is mainly controlled by the mode of p_s.

Figure 10 shows the continuum contributions to the spectral of the self-energy. The figure presents loop contributions expressed by the following combination $G_{\rm cont}(\omega)$:

$$G_{\rm cont}(\omega)=t_n^2[G_{h_s h_s^\dagger}(\omega)+G_{\psi_s\psi_s^\dagger}(\omega)+G_{\varphi_s\varphi_s^\dagger}(\omega)]$$
$$+2t_n^2\alpha_0[G_{\psi_s\psi_0^\dagger}(\omega)+G_{\varphi_s\varphi_0^\dagger}(\omega)]$$
$$+t_n^2\alpha_0^2[G_{h_0 h_0^\dagger}(\omega)+G_{\psi_0\psi_0^\dagger}(\omega)+G_{\varphi_0\varphi_0^\dagger}(\omega)]\ , \tag{3.8a}$$

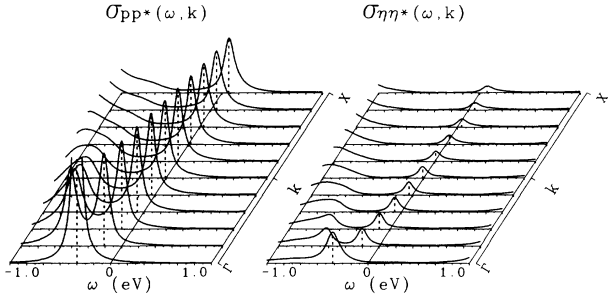

FIG. 7. Spectral density of p and d electrons for the case of the metallic phase [Fig. 6(c)].

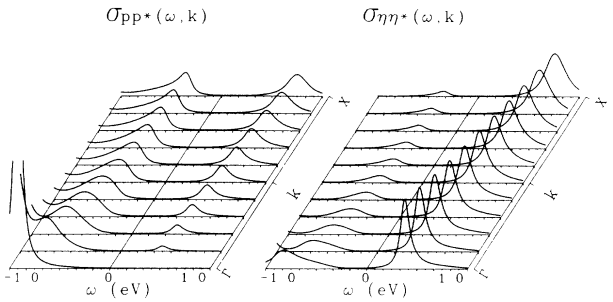

FIG. 8. Spectral density of p and d electrons for the case of the insulator phase [Fig. 6(a)].

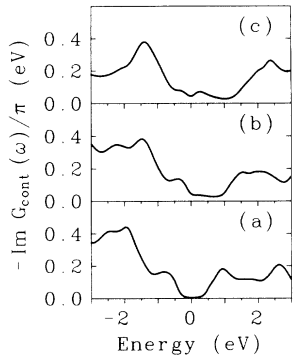

FIG. 10. Continuum contribution $G_{\mathrm{cont}}(\omega)$ to the self-energy of composite excitations. Parameters are the same as in Fig. 6.

which is the (p_s,p_s) component of δm after diagonalization of I (cf. Appendix B) and α_0 is defined as

$$\alpha_0=3b^2/(\chi_0-b^2)\ . \tag{3.8b}$$

In the present approximation, the intensity around the FL is considerably small compared with that of the higher-energy region, even after the large intensity of states develops at the FL, as seen in case (c) of Fig. 6 or 9. In order to investigate the behavior around the FL more accurately, it is necessary to treat the spectral whose main weights are around the FL. Such an improvement in the composite-operator approach is in progress.

As is seen in Table II, the mean field a_s is the one which changes largely by carrier doping. In order to clarify the physical meaning of a_s, let us consider p-hole densities C_s and C_t coupled with a Cu spin in spin singlet and triplet states, respectively, in the ground state. They are obtained from the relations

$$\langle (p^\dagger_\gamma \sigma_3 p_\gamma)^2(2-n_0)\rangle = C_s + C_t \tag{3.9a}$$

and

$$\langle p^\dagger_\gamma \sigma_3 p_\gamma n_3\rangle = -C_s+\tfrac{1}{3}C_t\ . \tag{3.9b}$$

Doping dependence of C_s and C_t is shown in Fig. 11. In the insulating case, $C_s/C_t\sim\frac{1}{3}$ reflecting the degeneracy of singlet and triplet states, which means that a p hole spin has little correlation with a Cu spin. In turn, C_s increases with the p-hole density n_h almost proportionally. This change is mostly controlled by a_s. The result indicates that p holes are mainly doped in the spin singlet state of p hole and Cu spins.

In Fig. 12, we show the spectrum of Cu-site spin (solid lines) and charge (dashed lines) local fluctuation in the following form:

$$\bar{\rho}^{\mu}_{00}(\omega)=\frac{1}{2}\frac{e^{\beta\omega}+1}{e^{\beta\omega}-1}\rho^{\mu}_{00}(\omega)/\langle(\delta n_\mu)^2\rangle\ , \tag{3.10}$$

which give the sum rule

$$\int d\omega\bar{\rho}^{\mu}_{00}(\omega)=1\ . \tag{3.11}$$

They are determined self-consistently with the electronic states of p, η, p_s, and p_0 shown in Figs. 6 and 9. Note that they are intrasite fluctuations. The doping dependences are quite different from each other between the spin and charge channel. In an insulating case (a), spin fluctuation has a sharp peak at $\omega=0$ and the weak spectrum at higher energy extending to 4 eV, while charge fluctuation has very little intensity at the low-energy region and a prominent peak around $\omega=1.8$ eV which is identified as the CT excitation. When holes are doped, the low-energy spin fluctuation around $\omega=0$ eV decreases and the weight is broadened up to the region of $\omega=0.5-1.5$ eV. On the other hand, the CT excitation is drastically reduced and the reduced peak shifts to a higher energy $\omega\sim1.8$ eV. Although the charge fluctua-

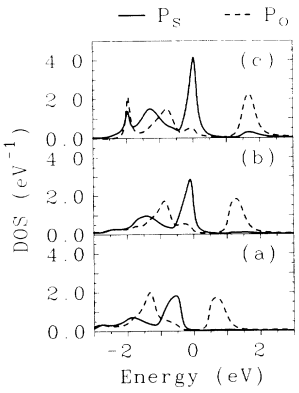

FIG. 9. Density of states for p_s [$\frac{1}{9}\sigma_{p_sp_s^\dagger}(\omega)$, solid line] and p_0 [$\sigma_{p_0p_0^\dagger}(\omega)$, dashed line]. Parameters are the same as in Fig. 6.

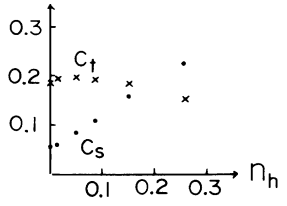

FIG. 11. p hole densities coupled with a Cu spin in singlet and triplet states in the ground state. Parameters are $t=0.5$ eV, $\Delta_0=1.2$ eV. The hole concentration n_h is calculated by changing ε_p.

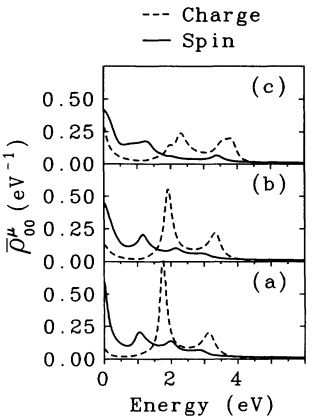

FIG. 12. Spectrums $\bar{\rho}^{\mu}_{00}(\omega)$ of Cu spin (solid line) and charge (dashed line) local fluctuations. Parameters are the same as in Fig. 6.

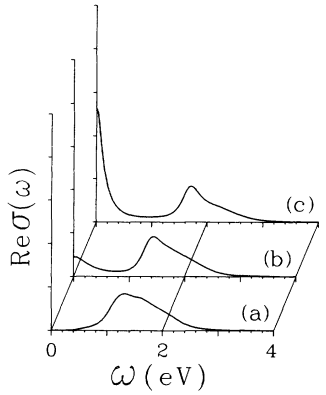

FIG. 13. Optical conductivity $\sigma(\omega)$. Parameters are the same as in Fig. 6.

tions shown in Fig. 12 are not directly related to the optical conductivity arising from the zero momentum transition, the tendency with doping is very similar to the results observed in the ir spectroscopy. Interestingly, the peak position of the CT excitation in cases (a) and (b) does not reflect directly the transition corresponding to the smallest energy gap expected from the one-particle density of states of p and d electrons shown in Fig. 6. Rather, the local charge fluctuation spectrum shows the charge-transfer gap formed between the p band below ε_p and the upper Hubbard band. The result can be understood in the following way. The energy gap in the charge fluctuation is formed by the p-hole–d-electron pair creation. In the local fluctuation, the pair creation inside a CuO_2 cluster is expected to dominate. When hole concentration is small, the total spin of the p-electron system in the CuO_2 cluster is nearly zero in the initial state of the transition, while in the final state the upper Hubbard level is occupied so that the spin of the Cu ion is zero. Therefore to the transition energy, the spin-dependent interaction does not operate, that is, the transition energy is nearly the difference between the energy of the upper Hubbard level and ε_p shifted only by the effect of charge fluctuation. When electrons gain itinerancy, intersite effects start to dominate and the intensity related to local transitions is rapidly decreased as is seen in Fig. 12(c). In this way, this phenomena can be understood as one of characteristic features of the highly correlated electron system. In optical conductivity, most of the contributions arise from the transfer interaction, and therefore at least two lattice sites are involved and the above-mentioned local constraint of spin freedom does not operate, that is, the observed gap in the insulator phase is more closer to that expected from the distribution of density of states as is shown in Fig. 13. Also, the transfer of the spectrum to a low-energy region is more drastic.

Next, we show the t dependence of the density of states in Fig. 14. We choose $t=0.5$ eV for cases (a)–(c) and $t=0.7$ eV for cases (d)–(f). The values of ε_p and ε_η are adjusted in such a way that the energy difference between the renormalized upper Hubbard level and the FL gives the same value in cases (a)–(c) and (d)–(f), and the hole density is about 0.22. One can see drastic changes of the spectral distribution. The accumulation of the density of states at the FL is more drastic for larger t by transferring intensities from the upper and lower portions of the spectrum. The bandwidths of the upper Hubbard band and the lower p band are also broadened. In order to understand the origin of the intensity transfer without destroying the three-peak structure, we present $-(1/\pi)\mathrm{Im}\Sigma_\eta(\omega)$ $[\equiv\sigma_\eta(\omega)]$ in Figs. 14(c) and 14(f), and $-(1/\pi)\mathrm{Im}\tilde{S}_{\eta\eta^\dagger}(\omega)$ $[\equiv\bar{\sigma}_\eta(\omega)]$ in Figs. 14(b) and 14(e). The vertical dashed lines show the position of the renormalized upper Hubbard level $\tilde{\varepsilon}_\eta$ $[\equiv\varepsilon_\eta-2bt_n/n]$. The peak structures in $-(1/\pi)\mathrm{Im}\Sigma_\eta(\omega)$ indicate the renor-

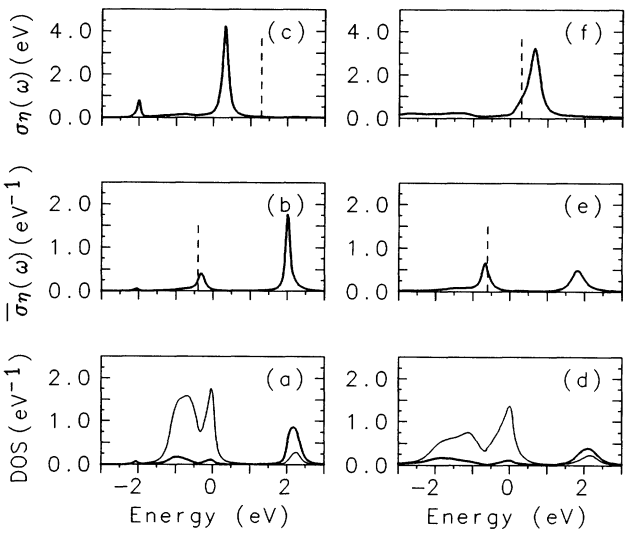

FIG. 14. Transfer t dependence of the density of states. (a)–(c) are for $t=0.5$ eV, and (d)–(f) are for $t=0.7$ eV. (a) and (d) show the full density of states, $\sigma_{\eta\eta^\dagger}(\omega)$ (bold solid line) and $\sigma_{pp^\dagger}(\omega)$ (fine solid line), (b) and (e) are for $\bar{\sigma}_\eta(\omega)$ $[=-(1/\pi)\mathrm{Im}\tilde{S}_{\eta\eta^\dagger}(\omega)]$ [cf. Eq. (3.21)] and (c) and (f) are for $\sigma_\eta(\omega)$ $[=-(1/\pi)\mathrm{Im}\Sigma_\eta(\omega)]$ [cf. Eq. (3.3)].

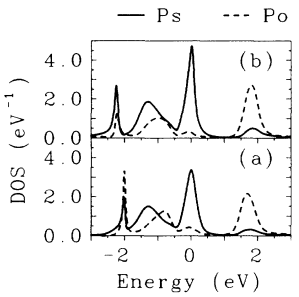

FIG. 15. Temperature dependence of the density of states for composite excitations p_s [$\frac{1}{9}\sigma_{p_s p_s\dagger}(\omega)$, solid line] and p_0 [$\sigma_{p_0 p_0\dagger}(\omega)$, dashed line]. Parameters are the same as in Fig. 6(c), and $T=0.06$ eV (a) and 0.03 eV (b).

malized positions of composite excitation induced by the mixing among p_0 and p_s. In $-(1/\pi)\mathrm{Im}\tilde{S}_{\eta\eta\dagger}(\omega)$, the intensity distributes according to the mixing between the renormalized upper Hubbard level and composite electronic levels. This structure is not the direct observable, but appears in the intermediate step of the mixing scheme. In the case of Fig. 14(c), $\tilde{\varepsilon}_\eta$ locates above the peak of $-(1/\pi)\mathrm{Im}\Sigma_\eta(\omega)$, while their positions are interchanged in the case of Fig. 14(f). This difference induces a drastic change of intensity distributions in Figs. 14(b) and 14(e); although the energies of peak positions are similar, their intensities are interchanged. This causes the large intensity transfer in the final density of states in Figs. 14(a) and 14(c). As can be seen in those figures, the density of states is very sensitive to the value of t. As t is larger, more intensity grows at the FL absorbing the weight from the bottom of the valence band and the upper Hubbard band. In addition, the larger t cases (a)–(c) are "qualitatively" different from cases (d)–(f) in the sense that the crossover happens concerning the level position of the pole at $\omega=\tilde{\varepsilon}_\eta$ and the peak of $-(1/\pi)\mathrm{Im}\Sigma_\eta(\omega)$, leading to the development of the state at the FL and the collapse of the upper Hubbard band. It shows similar electronic state obtained from a simple mixing of p- and renormalized d-electron levels. Experimentally, the collapse of the upper Hubbard band occurs by carrier doping. Our results of doping dependence

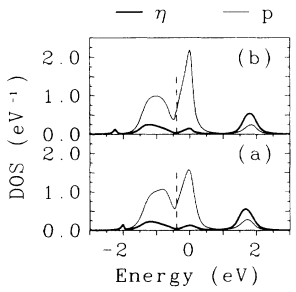

FIG. 16. Temperature dependence of the density of states for $\sigma_{pp\dagger}(\omega)$ (fine solid line) and $\sigma_{\eta\eta\dagger}(\omega)$ (bold solid line). Parameters are the same as in Fig. 15.

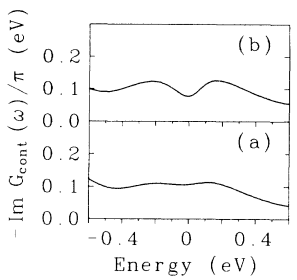

FIG. 17. Temperature dependence of the continuum contribution $G_{\mathrm{cont}}(\omega)$ to the self-energy of composite excitations. Parameters are the same as in Fig. 15.

with fixed t also show the reduction of the weight of the upper band, as seen in Fig. 6, which is qualitatively consistent with the experiments of XAS, EELS, and ir spectroscopy.

Finally, we show the temperature dependence. The state of p_s is enhanced and becomes more stable at the FL by lowering temperature. This is shown in Fig. 15: (a) $T=0.06$ eV and (b) $T=0.03$ eV. As a result, the density of states develops further by lowering temperature in p- and d-electron channels and the splitting of the valence band becomes clearer as seen in Fig. 16: (a) $T=0.06$ eV and (b) $T=0.03$ eV. In Fig. 17, we show the continuum given in Eq. (3.9). Cases (a) and (b) are for $T=0.06$ eV and $T=0.03$ eV, respectively. At lower temperature, the intensity of the continuum at the FL is decreases. This is the reason for an increase of the intensity at FL with lowering temperature.

IV. SUMMARY AND DISCUSSIONS

In this paper, we have analyzed the electronic state of the highly correlated p-d model in the viewpoint of the composite electronic excitation associated with the Cu-O bond. The composite operator is constructed as $p_\gamma \delta n_\mu$, and it is a combination of a relevant electron operator p_γ and an operator δn_μ describing the change of its environment. It is shown that the electronic state near the FL close to the metal-insulator transition of oxide cuprate is dominated by such composite excitations and that, due to the change of the renormalized levels and mixing strength, rapid modification of intensity distribution is induced. The mean-field result gives the approximate peak structure of intensity distribution, while the dynamical corrections work to pin the intensity at the FL and induce the transfer of state density to the FL from both upper and lower energy regions. The intensity transfer with carrier doping among levels, without modifying much of the energy distances, is one of the characteristic features in the metal-insulator transition of the highly correlated electron system, and the behavior is well understood by means of the mixing among composite electrons in the present analysis.

The characteristic features in the highly correlated electron system have been pointed out in this paper. One is qualitative changes of the electronic structure depending on the parameter t. There occurs the crossover from

the composite electron $p_\gamma \delta n_\mu$ domination to the restricted d-electron r denomination in the mixing scheme for the electronic state near the Fermi level. This may be interpreted as the change from a highly correlated electron state to a bandlike electron state. This change can be explained by the crossover between the levels of the renormalized composite electron level and the upper Hubbard level. The other is the behavior of the local fluctuations. Reflecting the highly correlated nature of the electron system, the pair creation energies are also very much modified due to the mutual interaction and they show different energies from the simple energy difference among one-particle states. However, the intensity corresponding to such transitions is rapidly decreased with increasing itinerancy, together with the domination of intraband transition processes.

The present analysis of the p-d-mixing model leads us to three important properties of the CuO_2 plane. (1) The electronic state near the FL may be sensitive to interactions which change properties of the Cu-O bond due to its composite character. The short distant Coulomb interaction between d and p electrons may induce stronger effects through fluctuations. Phonon effect related to Cu-O bonds may not be negligible. (2) There is a rapid change of the charge fluctuations. The charge fluctuation related to intrasite transfer is more enhanced in the low-energy region than the local one. Experimentally, it seems that superconductors show the maximum T_c when such rapid change occurs. It is still an open question whether or not this kind of rapid weight shift of charge fluctuations is related to some kind of electronic instability at the Fermi level. (3) There is a crossover from the composite excitation dominant mixing region to the simple p and upper Hubbard level mixing region. The itinerancy for composite excitations becomes largest just at the crossover point. It is also an interesting question whether or not such a crossover is related to the suppression of the superconductivity for the highly doped region.

ACKNOWLEDGMENTS

This work was supported by a Grant-in-Aid from the Ministry of Education, Science and Culture in Japan. The authors would like to express their thanks for valuable discussions to Dr. T. Koyama, Dr. S. Takahashi, and Mr. S. Ishihara. One of the authors (M.S.) would like to thank the NKK Corporation for financial support.

APPENDIX A: FORMULA TO OBTAIN $\mathrm{Im}J^{\mu}_{+\pm}(\omega)$

In order to calculate the dynamical correction $\delta M^{\mu}_{++}(\omega)$ and $\delta M^{\mu}_{+-}(\omega)$, we first evaluate the response function $J^{\mu}_{++}(\omega)$ and $J^{\mu}_{+-}(\omega)$ given in Eqs. (2.52a) and (2.52b) by one-loop approximation. The detailed expressions for $-(1/\pi)\mathrm{Im}J^{\mu}_{++}(\omega)$ and $-(1/\pi)\mathrm{Im}J^{\mu}_{+-}(\omega)$ are as follows. Note that $J^{1}_{+\pm}(\omega)=J^{2}_{+\pm}(\omega)=J^{3}_{+\pm}(\omega) \equiv J^{s}_{+\pm}(\omega)$. We have

$$
\begin{aligned}
-\frac{1}{\pi}\mathrm{Im}J^{0}_{++}(\omega)=2t_n^2\int d\nu[f_F(\nu)+f_F(\nu+\omega)]
\times\Bigg[&\sigma_{p_\gamma p_\gamma^\dagger}(\nu+\omega)\sigma_{p_\gamma p_\gamma^\dagger}(\nu)+\frac{1}{n^2}\{[\sigma_{p_0 p_0^\dagger}(\nu+\omega)-2\sigma_{p_0 p_s^\dagger}(\nu+\omega)+\sigma_{p_s p_s^\dagger}(\nu+\omega)]\sigma_{p_\gamma p_\gamma^\dagger}(\nu)\\
&+\sigma_{p_\gamma p_\gamma^\dagger}(\nu+\omega)[\sigma_{p_0 p_0^\dagger}(\nu)-2\sigma_{p_0 p_s^\dagger}(\nu)+\sigma_{p_s p_s^\dagger}(\nu)]\\
&+2[\sigma_{p_0 p_\gamma^\dagger}(\nu+\omega)-\sigma_{p_s p_\gamma^\dagger}(\nu+\omega)][\sigma_{p_0 p_\gamma^\dagger}(\nu)-\sigma_{p_s p_\gamma^\dagger}(\nu)]\\
&-[g^0_{p_\gamma p_\gamma^\dagger}(\nu+\omega)+3g^s_{p_\gamma p_\gamma^\dagger}(\nu+\omega)]\sigma_{p_\gamma p_\gamma^\dagger}(\nu)\}\\
&+\sigma_{rr^\dagger}(\nu+\omega)\sigma_{r_{\gamma_1^2} r^\dagger_{\gamma_1^2}}(\nu)+\frac{2}{n}\{[\sigma_{p_0 p_\gamma^\dagger}(\nu+\omega)-\sigma_{p_s p_\gamma^\dagger}(\nu+\omega)]\sigma_{p_\gamma p_\gamma^\dagger}(\nu)\\
&\qquad+\sigma_{p_\gamma p_\gamma^\dagger}(\nu+\omega)[\sigma_{p_0 p_\gamma^\dagger}(\nu)-\sigma_{p_s p_\gamma^\dagger}(\nu)]\}\\
&-2\sigma_{p_\gamma r^\dagger}(\nu+\omega)\sigma_{p_\gamma r\gamma_1^{2\dagger}}(\nu)-\frac{2}{n}\{[\sigma_{p_0 r^\dagger}(\nu+\omega)-\sigma_{p_s r^\dagger}(\nu+\omega)]\sigma_{p_\gamma r^\dagger_{\gamma_1^2}}(\nu)\\
&\qquad+\sigma_{p_\gamma r^\dagger}(\nu+\omega)[\sigma_{p_0 r^\dagger_{\gamma_1^2}}(\nu)-\sigma_{p_s r^\dagger_{\gamma_1^2}}(\nu)]\}\Bigg],
\end{aligned}
\tag{A1}
$$

$$-\frac{1}{\pi}\,\mathrm{Im}J^{s}_{++}(\omega)=2t_n^2\int d\nu[f_F(\nu)+f_F(\nu+\omega)]$$
$$\times\Bigg[\sigma_{p_\gamma p^\dagger_\gamma}(\nu+\omega)\sigma_{p_\gamma p^\dagger_\gamma}(\nu)+\frac{1}{n^2}\{[\sigma_{p_0p^\dagger_0}(\nu+\omega)-2\sigma_{p_0p^\dagger_s}(\nu+\omega)+\sigma_{p_0p^\dagger_s}(\nu+\omega)]\sigma_{p_\gamma p^\dagger_\gamma}(\nu)$$
$$+2[\sigma_{p_0p^\dagger_\gamma}(\nu+\omega)-\sigma_{p_sp^\dagger_\gamma}(\nu+\omega)][\sigma_{p_0p^\dagger_\gamma}(\nu)+\tfrac{1}{3}\sigma_{p_sp^\dagger_\gamma}(\nu)]$$
$$+\sigma_{p_\gamma p^\dagger_\gamma}(\nu+\omega)[\sigma_{p_0p^\dagger_0}(\nu)+\tfrac{2}{3}\sigma_{p_0p^\dagger_s}(\nu)+\frac{1}{9}\sigma_{p_sp^\dagger_s}(\nu)]$$
$$-[g^0_{p_\gamma p^\dagger_\gamma}(\nu+\omega)+\tfrac{1}{3}g^s_{p_\gamma p^\dagger_\gamma}(\nu+\omega)]\sigma_{p_\gamma p^\dagger_\gamma}(\nu)\}$$
$$+\sigma_{rr^\dagger}(\nu+\omega)\sigma_{r_{\gamma_1^2}r^\dagger_{\gamma_1^2}}(\nu)+\frac{2}{n}\{[\sigma_{p_0p^\dagger_\gamma}(\nu+\omega)-\sigma_{p_sp^\dagger_\gamma}(\nu+\omega)]\sigma_{p_\gamma p^\dagger_\gamma}(\nu)$$
$$+\sigma_{p_\gamma p^\dagger_\gamma}(\nu+\omega)[\sigma_{p_0p^\dagger_\gamma}(\nu)+\tfrac{1}{3}\sigma_{p_sp^\dagger_\gamma}(\nu)]\}$$
$$-2\sigma_{p_\gamma r^\dagger}(\nu+\omega)\sigma_{p_\gamma r^\dagger_{\gamma_1^2}}(\nu)-\frac{2}{n}\{[\sigma_{p_0r^\dagger}(\nu+\omega)-\sigma_{p_sr^\dagger}(\nu+\omega)]\sigma_{p_\gamma r^\dagger_{\gamma_1^2}}(\nu)$$
$$+\sigma_{p_\gamma r^\dagger}(\nu+\omega)[\sigma_{p_0r^\dagger_{\gamma_1^2}}(\nu)+\tfrac{1}{3}\sigma_{p_sr^\dagger_{\gamma_1^2}}(\nu)]\}\Bigg],\tag{A2}$$

$$-\frac{1}{\pi}\,\mathrm{Im}J^{0}_{+-}(\omega)=-2t_n^2\int d\nu[f_F(\nu)+f_F(\nu+\omega)]$$
$$\times\Bigg[\sigma_{p_\gamma p^\dagger_\gamma}(\nu+\omega)\sigma_{p_\gamma p^\dagger_\gamma}(\nu)+\frac{1}{n^2}\{+[\sigma_{p_0p^\dagger_0}(\nu+\omega)-2\sigma_{p_sp^\dagger_s}(\nu+\omega)+\sigma_{p_sp^\dagger_s}(\nu+\omega)]\sigma_{p_\gamma p^\dagger_\gamma}(\nu)$$
$$+\sigma_{p_\gamma p^\dagger_\gamma}(\nu+\omega)[\sigma_{p_0p^\dagger_0}(\nu)-2\sigma_{p_0p^\dagger_s}(\nu)+\sigma_{p_sp^\dagger_s}(\nu)]$$
$$+2[\sigma_{p_0p^\dagger_\gamma}(\nu+\omega)-\sigma_{p_sp^\dagger_\gamma}(\nu+\omega)][\sigma_{p_0p^\dagger_\gamma}(\nu)-\sigma_{p_sp^\dagger_\gamma}(\nu)]$$
$$-[g^0_{p_\gamma p^\dagger_\gamma}(\nu+\omega)+3g^s_{p_\gamma p^\dagger_\gamma}(\nu+\omega)]\sigma_{p_\gamma p^\dagger_\gamma}(\nu)\}$$
$$+\sigma_{rr^\dagger_{\gamma_1^2}}(\nu+\omega)\sigma_{rr^\dagger_{\gamma_1^2}}(\nu)+\frac{2}{n}\{[\sigma_{p_0p^\dagger_\gamma}(\nu+\omega)-\sigma_{p_sp^\dagger_\gamma}(\nu+\omega)]\sigma_{p_\gamma p^\dagger_\gamma}(\nu)$$
$$+\sigma_{p_\gamma p^\dagger_\gamma}(\nu+\omega)[\sigma_{p_0p^\dagger_\gamma}(\nu)-\sigma_{p_sp^\dagger_\gamma}(\nu)]\}$$
$$-2[\sigma_{p_\gamma r^\dagger}(\nu+\omega)\sigma_{p_\gamma r^\dagger_{\gamma_1^2}}(\nu)+\sigma_{p_\gamma r_{\gamma_1^2}}(\omega+\nu)\sigma_{p_\gamma r^\dagger}(\nu)]$$
$$-\frac{2}{n}\{[\sigma_{p_0r^\dagger_{\gamma_1^2}}(\nu+\omega)-\sigma_{p_sr^\dagger_{\gamma_1^2}}(\nu+\omega)]\sigma_{p_\gamma r^\dagger}(\nu)$$
$$+\sigma_{p_\gamma r^\dagger}(\nu+\omega)[\sigma_{p_0r^\dagger_{\gamma_1^2}}(\nu)-\sigma_{p_sr^\dagger_{\gamma_1^2}}(\nu)]$$
$$+[\sigma_{p_0r^\dagger}(\nu+\omega)-\sigma_{p_sr^\dagger}(\nu+\omega)]\sigma_{p_\gamma r^\dagger_{\gamma_1^2}}(\nu)$$
$$+\sigma_{p_\gamma r^\dagger_{\gamma_1^2}}(\nu+\omega)[\sigma_{p_0r^\dagger}(\nu)-\sigma_{p_sr^\dagger}(\nu)]\}\Bigg],\tag{A3}$$

$$-\frac{1}{\pi}\mathrm{Im}J^{s}_{+-}(\omega)=-2t_n^2\int d\nu[f_F(\nu)+f_F(\nu+\omega)]$$
$$\times\Big[\sigma_{p_\gamma p^\dagger_\gamma}(\nu+\omega)\sigma_{p_\gamma p^\dagger_\gamma}(\nu)+\frac{1}{n^2}\{+[\sigma_{p_0 p^\dagger_\gamma}(\nu+\omega)-\sigma_{p_s p^\dagger_\gamma}(\nu+\omega)][\sigma_{p_0 p^\dagger_\gamma}(\nu)-\sigma_{p_s p^\dagger_\gamma}(\nu)]$$
$$+[\sigma_{p_0 p^\dagger_0}(\nu+\omega)-\tfrac{2}{3}\sigma_{p_0 p^\dagger_s}(\nu+\omega)-\tfrac{1}{3}\sigma_{p_s p^\dagger_s}(\nu+\omega)]\sigma_{p_\gamma p^\dagger_\gamma}(\nu)$$
$$+\sigma_{p_\gamma p^\dagger_\gamma}(\nu+\omega)[\sigma_{p_0 p^\dagger_0}(\nu)-\tfrac{2}{3}\sigma_{p_0 p^\dagger_s}(\nu)-\tfrac{1}{3}\sigma_{p_s p^\dagger_s}(\nu)]$$
$$+[\sigma_{p_0 p^\dagger_\gamma}(\nu+\omega)+\tfrac{1}{3}\sigma_{p_s p^\dagger_\gamma}(\nu+\omega)][\sigma_{p_0 p^\dagger_\gamma}(\nu)+\tfrac{1}{3}\sigma_{p_s p^\dagger_\gamma}(\nu)]$$
$$-[g^0_{p_\gamma p^\dagger_\gamma}(\nu+\omega)-g^s_{p_\gamma p^\dagger_\gamma}(\nu+\omega)]\sigma_{p_\gamma p^\dagger_\gamma}(\nu)\}$$
$$+\sigma_{rr^\dagger_{\gamma_1^2}}(\nu+\omega)\sigma_{rr^\dagger_{\gamma_1^2}}(\nu)+\frac{2}{n}\{[\sigma_{p_0 p^\dagger_\gamma}(\nu+\omega)-\tfrac{1}{3}\sigma_{p_s p^\dagger_\gamma}(\nu+\omega)]\sigma_{p_\gamma p^\dagger_\gamma}(\nu)$$
$$+\sigma_{p_\gamma p^\dagger_\gamma}(\nu+\omega)[\sigma_{p_0 p^\dagger_\gamma}(\nu)-\tfrac{1}{3}\sigma_{p_s p^\dagger_\gamma}(\nu)]\}$$
$$-2[\sigma_{p_\gamma r^\dagger}(\nu+\omega)\sigma_{p_\gamma r^\dagger_{\gamma_1^2}}(\nu)+\sigma_{p_\gamma r^\dagger_{\gamma_1^2}}(\omega+\nu)\sigma_{p_\gamma r^\dagger}(\nu)]$$
$$-\frac{2}{n}\{[\sigma_{p_0 r^\dagger_{\gamma_1^2}}(\nu+\omega)-\sigma_{p_s r^\dagger_{\gamma_1^2}}(\nu+\omega)]\sigma_{p_\gamma r^\dagger}(\nu)$$
$$+\sigma_{p_\gamma r^\dagger}(\nu+\omega)[\sigma_{p_0 r^\dagger_{\gamma_1^2}}(\nu)-\sigma_{p_s r^\dagger_{\gamma_1^2}}(\nu)]$$
$$+[\sigma_{p_0 r^\dagger}(\nu+\omega)+\tfrac{1}{3}\sigma_{p_s r^\dagger}(\nu+\omega)]\sigma_{p_\gamma r^\dagger_{\gamma_1^2}}(\nu)$$
$$+\sigma_{p_\gamma r^\dagger_{\gamma_1^2}}(\nu+\omega)[\sigma_{p_0 r^\dagger}(\nu)+\tfrac{1}{3}\sigma_{p_s r^\dagger}(\nu)]\}\Big]\,, \tag{A4}$$

where

$$g^{\mu}_{p_\gamma p^\dagger_\gamma}(\omega)=\int d\nu[f_F(\nu-\omega)f_F(-\nu)+f_F(\omega-\nu)f_F(\nu)]$$
$$\times\bar{\rho}^{\mu}_{00}(\omega-\nu)\sigma_{p_\gamma p^\dagger_\gamma}(\nu) \tag{A5a}$$

and

$$g^{s}_{p_\gamma p^\dagger_\gamma}(\omega)\equiv g^{1}_{p_\gamma p^\dagger_\gamma}(\omega)=g^{2}_{p_\gamma p^\dagger_\gamma}(\omega)=g^{3}_{p_\gamma p^\dagger_\gamma}(\omega)\,. \tag{A5b}$$

APPENDIX B: DIAGONALIZATION OF $I(\mathbf{k})$ AND THE FUNCTION $\Sigma_\eta(\omega,\mathbf{k})$

As seen in Eq. (2.24), the matrix $I(\mathbf{k})$ has off-diagonal components. In actual calculation, it is more convenient to construct the orthogonalized set $\{\Psi_n\}$ from $\{\psi_n\}$ in such a way that off-diagonal components of $\langle\{\Psi_n(\mathbf{x}),\Psi^\dagger_n(\mathbf{y})\}\rangle$ are all zero. We transform $\{\psi_n(\mathbf{x})\}$ to $\{\Psi_n(\mathbf{x})\}$ by

$$\Psi_n(\mathbf{x})=\psi_n(\mathbf{x})-\sum_{m=1}^{n-1}\alpha_{nm}(-i\nabla)\psi_m(\mathbf{x})\,, \tag{B1}$$

where coefficients $\alpha_{nm}(-i\nabla)$ are determined to satisfy components of $\langle\{\Psi_n(\mathbf{x}),\Psi^\dagger_n(\mathbf{y})\}\rangle$,

$$\langle\{\Psi_n(\mathbf{x}),\Psi^\dagger_l(\mathbf{y})\}\rangle=\delta_{nl}\langle\{\Psi_n(\mathbf{x}),\Psi^\dagger_n(\mathbf{y})\}\rangle\,. \tag{B2}$$

By defining

$$I'_n(\mathbf{x}-\mathbf{y})=\langle\{\Psi_n(\mathbf{x}),\Psi^\dagger_n(\mathbf{y})\}\rangle\,, \tag{B3}$$

the recurrence formulas are obtained from Eqs. (B1) and (B2),

$$I'_n(\mathbf{k})=I_{nn}(\mathbf{k})-\sum_{m=1}^{n-1}\alpha^*_{nm}(\mathbf{k})I_{nm}(\mathbf{k})\,, \tag{B4}$$

$$\alpha_{nl}(\mathbf{k})=\left[I_{nl}(\mathbf{k})-\sum_{m=1}^{l-1}\alpha^*_{lm}(\mathbf{k})\alpha_{nm}(\mathbf{k})I'_m(\mathbf{k})\right]\Big/I'_n(\mathbf{k})\,. \tag{B5}$$

Now the equation of motion (2.12) is transformed to

$$i\frac{\partial}{\partial t}\Psi_n(x)=J_n(x)\,, \tag{B6}$$

where

$$J_n(\mathbf{x})=\psi_n(\mathbf{x})-\sum_{m=1}^{n-1}\alpha_{nm}(-i\nabla)J_m(\mathbf{x})\,. \tag{B7}$$

Then the generalized mean field $m_0(\mathbf{x}-\mathbf{y})$ and the dynamical correction $\delta m(x-y)$ are transformed to

$M_0(\mathbf{x}-\mathbf{y})$ and $\delta M(x-y)$, respectively, by the recurrence formula,

$$M_{nm}=m_{nm}-\sum_{l=1}^{n-1}\alpha_{nl}(\mathbf{k})M_{lm}-\sum_{l=1}^{m-1}\alpha^{*}_{ml}(\mathbf{k})M_{nl}-\sum_{l'=1}^{m-1}\sum_{l=1}^{n-1}\alpha^{*}_{ml'}(\mathbf{k})\alpha_{nl}(\mathbf{k})M_{ll'}\ , \tag{B8}$$

where M is either $M(\mathbf{k})$or $\delta M(\omega,\mathbf{k})$ and m is either $m(\mathbf{k})$ or $\delta m(\omega,\mathbf{k})$. The Green function of $\{\Psi_n\}$ is expressed as

$$S_{\Psi\Psi^{\dagger}}(\omega,\mathbf{k})=I'(\mathbf{k})\left[\frac{1}{\omega I'(\mathbf{k})-M(\mathbf{k})-\delta M(\omega,\mathbf{k})}\right]I'(\mathbf{k})\ . \tag{B9}$$

By dividing 4×4 matrices into 2×2 submatrices as

$$S_{\Psi\Psi^{\dagger}}\equiv\begin{bmatrix}S_1 & S_2\\ S_3 & S_4\end{bmatrix}\ , \tag{B10a}$$

$$I'\equiv\begin{bmatrix}I'_A & 0\\ 0 & I'_D\end{bmatrix}\ , \tag{B10b}$$

and

$$(M_0+\delta M)I'^{-1}\equiv\begin{bmatrix}A & B\\ C & D\end{bmatrix}\ , \tag{B10c}$$

$S_{\Psi\Psi^{\dagger}}$ is obtained in the form

$$S_1=\left[\omega-A-B\frac{1}{\omega-D}C\right]^{-1}I'_A\ , \tag{B11a}$$

$$S_2=\left[\omega-A-B\frac{1}{\omega-D}C\right]^{-1}B\frac{1}{\omega-D}I'_D\ , \tag{B11b}$$

$$S_3=S_2^{\dagger}\ , \tag{B11c}$$

$$S_4=\frac{1}{\omega-D}I'_D+\frac{1}{\omega-D}CS_2\ . \tag{B11d}$$

The 2×2 submatrices A, B, C, and D are given as

$$A=\begin{bmatrix}\varepsilon_p & t_n\gamma^2(\mathbf{k})\\ t_n & \tilde{\varepsilon}_\eta\end{bmatrix}\ , \tag{B12a}$$

$$B=\frac{t_n}{n}\begin{bmatrix}0 & 0\\ b_1(\mathbf{k}) & b_2\end{bmatrix}\ , \tag{B12b}$$

$$C=\frac{t_n}{n}\begin{bmatrix}0 & c_1(\mathbf{k})\\ 0 & c_2(\mathbf{k})\end{bmatrix}\ , \tag{B12c}$$

$$D=\begin{bmatrix}[M(\mathbf{k})+\delta M(\omega,\mathbf{k})]_{33}/I'_3(\mathbf{k}) & [M(\mathbf{k})+\delta M(\omega,\mathbf{k})]_{34}/I'_4(\mathbf{k})\\ [M(\mathbf{k})+\delta M(\omega,\mathbf{k})]_{34}/I'_3(\mathbf{k}) & [M(\mathbf{k})+\delta M(\omega,\mathbf{k})]_{44}/I'_4(\mathbf{k})\end{bmatrix}\equiv\begin{bmatrix}d_1(\omega,\mathbf{k}) & d_2(\omega,\mathbf{k})\\ d_3(\omega,\mathbf{k}) & d_4(\omega,\mathbf{k})\end{bmatrix}\ , \tag{B12d}$$

where

$$b_1(\mathbf{k})=1+3b^2/I'_3(\mathbf{k}),\quad b_2=-1\ , \tag{B13a}$$

$$c_1(\mathbf{k})=b_1(\mathbf{k})I'_3(\mathbf{k}),\quad c_2(\mathbf{k})=I'_4(\mathbf{k})\ . \tag{B13b}$$

The effects of composite electronic excitations to the p and d electrons appear in the form $B(\omega-D)^{-1}C$ in Eq. (B11a), which is written as

$$B\frac{1}{\omega-D}C=\begin{bmatrix}0 & 0\\ 0 & \Sigma_\eta(\omega,\mathbf{k})\end{bmatrix} \tag{B14}$$

and

$$\Sigma_\eta(\omega,\mathbf{k})=\left[\frac{t_n}{n}\right]^2\{b_1(\mathbf{k})[(\omega-d_4(\omega,\mathbf{k}))c_1(\mathbf{k})+d_2(\omega,\mathbf{k})c_2(\mathbf{k})]+b_2(\mathbf{k})[(\omega-d_1(\omega,\mathbf{k}))c_2(\mathbf{k})+d_3(\omega,\mathbf{k})c_1(\mathbf{k})]\}\times\{(\omega-d_1(\omega,\mathbf{k}))(\omega-d_4(\omega,\mathbf{k}))-d_2(\omega,\mathbf{k})d_3(\omega,\mathbf{k})\}^{-1}\ . \tag{B15}$$

The function $\Sigma_\eta(\omega,\mathbf{k})$ appears in the expression of one-p-electron irreducible part $\tilde{S}_{\eta\eta^{\dagger}}(\omega,\mathbf{k})$, i.e., Eq. (3.3).

[1]See, for example, as a general review, *Strong Correlation and Superconductivity*, edited by H. Fukuyama, S. Maekawa, and A. P. Malozemoff (Springer-Verlag, Berlin, 1989).

[2]J. B. Torrance, T. Tokura, A. I. Nazzal, A. Bezinge, T. C. Huang, and S. S. P. Parkin, Phys. Rev. Lett. **61**, 1127 (1988); J. B. Torrance, A. Bezinge, A. I. Nazzal, T. C. Huang, S. S. P. Parkin, D. T. Keane, S. J. La Placa, P. M. Horn, and G. A. Held, Phys. Rev. B **40**, 8872 (1989).

[3]Zhi-xun Shen, J. W. Allen, J. J. Yek, J.-S. Kang, W. Ellis, W. Spicer, I. Lindeau, W. B. Maple, Y. D. Dalichaouch, M. S. Torikachoili, J. Z. Sun, and T. H. Geballe, Phys. Rev. B **36**, 8414 (1987).

[4]A. Fujimori, E. Takayama-Muromachi, Y. Uchida, and B. Okai, Phys. Rev. B **35**, 8814 (1987).

[5]R. L. Kurtz, R. L. Stockbauer, D. Mueller, A. Shih, L. E. Toth, M. Osofsky, and St. A. Wolf, Phys. Rev. B **35**, 8818 (1987).

[6]D. van der Marel, J. van Elp, G. A. Sawatzky, and D. Heitmann, Phys. Rev. B **35**, 8818 (1987).

[7]Y. Gao, T. J. Wagener, J. H. Weaver, A. J. Arko, B. Flandermeyer, and D. W. Capone II, Phys. Rev. B **36**, 3971 (1987).

[8]T. Takahashi, H. Matsuyama, H. Katayama-Yoshida, Y. Okabe, S. Hosoya, K. Seki, H. Fujimoto, M. Sato, and H. Inokuchi, Nature (London) **334**, 691 (1988); Phys. Rev. B **39**, 6636 (1989).

[9]J. H. Weaver, H. M. Meyer III, T. J. Wagener, D. M. Hill, Y. Gao, D. Peterson, Z. Fisk, and A. J. Arko, Phys. Rev. B **38**, 4668 (1988).

[10]A. J. Viescas, J. M. Tranquada, A. R. Moodenbaugh, and P. D. Johnson, Phys. Rev. B **37**, 3738 (1988).

[11]A. J. Arko, R. S. List, R. J. Barlett, S.-W. Cheong, Z. Fisk, J. D. Thompson, C. G. Olson, A.-B. Yang, R. Liu, C. Gu, B. W. Veal, J. Z. Liu, A. P. Paulikas, K. Vandervoort, H. Claus, J. C. Campuzzano, J. E. Scirber, and N. D. Shinn, Phys. Rev. B **40**, 2268 (1989).

[12]T. J. Wagener, H. M. Mayer III, Yongjun Hu, M. B. Jost, J. H. Weaver, and K. C. Goretta, Phys. Rev. B **41**, 4201 (1990).

[13]J. W. Allen, C. G. Olson, M. B. Maple, J.-S. Kang, L. Z. Liu, J.-H. Park, R. O. Anderson, W. P. Ellis, J. T. Markert, Y. Dalichaouch, and R. Liu, Phys. Rev. Lett. **64**, 595 (1990).

[14]T. Suzuki, M. Nagoshi, Y. Fukuda, K. Oh-ishi, Y. Syono, and M. Tachiki, Phys. Rev. B **42**, 4263 (1990).

[15]T. Takahashi, S. Suzuki, T. Kusunoki, S. Sato, H. Katayama-Yoshida, A. Yamanaka F. Minami, and S. Takekawa, Physica C **185-189**, 1057 (1991).

[16]C. G. Olsen, R. Liu, A.-B. Yang, D. W. Lynch, A. J. Arko, R. S. List, B. W. Veal, Y. C. Chang, P. Z. Jiang, and A. P. Paulikas, Science **245**, 731 (1989).

[17]R. Manzke, T. Buslap, R. Claessen, and J. Fink, Europhys. Lett. **9**, 477 (1989); R. Manzke, T. Bulaps, R. Claessen, M. Skibowski, and J. Fink, Physica C **162–164**, 1381 (1989).

[18]J. C. Campuzzano, G. Jennings, M. Faiz, L. Beaulaigue, B. W. Veal, J. Z. Liu, A. P. Paulikas, K. Vandervoort, H. Claus, R. S. List, A. J. Arko, and R. J. Bartlett, Phys. Rev. Lett. **64**, 2308 (1990).

[19]Y. Sakisaka, T. Murayama, Y. Morikawa, H. Kato, K. Enomoto, M. Okusawa, Y. Aiura, H. Ynashima, T. Terashima, Y. Bando, K. Iijima, K. Yamamoto, and K. Hirata, Phys. Rev. B **42**, 4189 (1990).

[20]T. Kusunoki, T. Takahashi, S. Sato, H. Katayama-Yoshida, K. Kamiya, and H. Inokuchi, Physica C **185-189**, 1045 (1991).

[21]A. Bianconi, M. De Santis, A. Di Cicco, A. M. Flank, A. Fontaine, P. Legarde, H. Katayama-Yoshida, A. Kotani, and Marcelli, Phys. Rev. B **38**, 7196 (1988).

[22]M. Abbate, M. Sacchi, J. J. Wunk, L. W. M. Schreurs, Y. S. Wang, R. Lof, and J. C. Fuggle, Phys. Rev. B **42**, 7914 (1990).

[23]S. Suzuki, T. Takahashi, T. Kusunoki, T. Morikawa, S. Sato, H. Katayama-Yoshida, A. Yamanaka, F. Minami, and S. Takekawa, Phys. Rev. B **44**, 5381 (1991).

[24]H. Matsuyama, T. Takahashi, H. Katayama-Yoshida, Y. Okabe, T. Kashiwamura, and S. Sato, Physica C **160**, 567 (1989).

[25]C. T. Chen, F. Sette, Y. Ma, M. S. Hybertsen, E. B. Stechel, W. M. C. Foulkes, M. Schluter, S.-W. Cheong, A. S. Cooper, L. W. Rupp, Jr., B. Batlogg, Y. L. Soo, Z. H. Ming, A. Krol, and Y. H. Kao, Phys. Rev. Lett. **66**, 104 (1991).

[26]N. Nücker, J. Fink, B. Renker, D. Ewert, C. Politis, P. J. W. Weijs, and J. C. Fuggle, Z. Phys. B **67**, 497 (1987); N. Nücker, J. Fink, J. C. Fuggle, P. J. Durham, and W. M. Temmerman, Phys. Rev. B **37**, 5158 (1988); N. Nücker, H. Romberg, X. X. Xi, J. Fink, B. Gegenheimer, and Z. X. Zhao, *ibid.* **39**, 6619 (1989).

[27]H. Romberg, M. Alexander, N. Nücker, P. Adelmann, and J. Fink, Phys. Rev. B **42**, 8768 (1990).

[28]M. Alexander, H. Romberg, N. Nücker, P. Adelmann, J. Fink, J. T. Markert, M. B. Maple, S. Uchida, H. Takagi, Y. Tokura, A. C. W. P. James, and D. W. Murphy, Phys. Rev. B **43**, 333 (1991).

[29]S. Uchida, T. Ido, H. Takagi, T. Arima, Y. Tokura, and S. Tajima, Phys. Rev. B **43**, 7942 (1991).

[30]J. Orenstein, G. A. Thomas, A. J. Mills, S. L. Cooper, D. H. Rapkine, T. Timusk, L. F. Schneemeyer, and J. V. Waszczak, Phys. Rev. B **42**, 6342 (1990).

[31]I. Terasaki, T. Nakahashi, S. Takebayashi, A. Maeda, and K. Uchinokura, Physica C **165**, 152 (1990).

[32]A. Maeda, M. Hase, I. Tsukada, K. Noda, S. Takebayashi, and K. Uchinokura, Physica C **165**, 152 (1990).

[33]S. L. Cooper, G. A. Thomas, A. J. Mills, P. E. Sulewski, J. Orenstein, D. H. Rapkine, S. W. Cheong, and P. L. Trevor, Phys. Rev. B **42**, 10 785 (1990).

[34]Y. Tokura, S. Koshihara, T. Arima, H. Takagi, S. Ishibashi, T. Ido, and S. Uchida, Phys. Rev. B **41**, 11 675 (1990).

[35]S. Tajima, S. Uchida, S. Ishibashi, T. Ido, H. Takagi, T. Arima, and Y. Tokura, Physica C **168**, 117 (1990).

[36]T. Arima, K. Kikuchi, M. Kasuya, S. Koshihara, and Y. Tokura, Phys. Rev. B **44**, 917 (1991).

[37]F. Mila, Phys. Rev. B **38**, 11 358 (1988).

[38]A. K. McMahan, R. M. Martin, and S. Satpathy, Phys. Rev. B **38**, 6650 (1988).

[39]M. S. Hyberstsen and M. Schlüter, Phys. Rev. B **39**, 9028 (1989).

[40]A. Kotani, in *Strong Correlation and Superconductivity*, edited by H. Fukuyama, S. Maekawa, and A. P. Malozemoff (Springer-Verlag, Berlin, 1989), p. 77.

[41]C. M. Varma, S. Schmitt-Rink, and E. Abrahams, Solid State Commun. **621**, 681 (1987).

[42]T. Koyama, M. Sasaki, and M. Tachiki, Physica C **153–155**, 1317 (1988).

[43]P. B. Littlewood, C. M. Varma, S. Schmitt-Rink, and E. Abrahams, Phys. Rev. B **39**, 12 371 (1989).

[44]R. Putz, G. Dopf, B. Ehlers, L. Lilly, A. Muramatsu, and W. Hanke, Phys. Rev. B **41**, 853 (1990).

[45]Z. Tesanovic, A. R. Bishop, and R. L. Martin, Solid State Commun. **621**, 681 (1987).

[46]P. B. Littlewood, Phys. Rev. B **42**, 10 075 (1990).

[47]R. T. Schüttler, Phys. Rev. B **38**, 2854 (1988).

[48]V. J. Emery, Phys. Rev. Lett. **58**, 2794 (1987).

[49]D. M. Newns, M. Dasolt, and P. C. Pattnaik, Phys. Rev. B **38**, 6513 (1988).

[50]P. C. Pattnaik and D. M. Newns, Phys. Rev. B **41**, 880 (1990).
[51]H. Matsumoto, M. Sasaki, and M. Tachiki, Solid State Commun. **71**, 829 (1989).
[52]H. Matsumoto, M. Sasaki, and M. Tachiki, Phys. Rev. B **43**, 10 247 (1991).
[53]H. Matsumoto, M. Sasaki, and M. Tachiki, Phys. Rev. B **43**, 10 264 (1991).
[54]H. Jichu, T. Matsuura, and Y. Kuroda, J. Phys. Soc. Jpn. **60**, 2269 (1991).
[55]D. S. Hirashima, Y. Ono, K. Miura, T. Matsuura, and H. Jichu, J. Phys. Soc. Jpn. **60**, 2269 (1991).
[56]J. E. Hirsh, Phys. Rev. B **35**, 8726 (1987).
[57]J. R. Schrieffer, X. G. Wen, and S. C. Zhang, Phys. Rev. Lett. **60**, 944 (1988); A. Kampf and J. R. Schrieffer, Phys. Rev. B **41**, 6399 (1990).
[58]T. Moriya, Y. Takahashi, and K. Ueda, J. Phys. Soc. Jpn. **59**, 2905 (1990).
[59]F. C. Zhang and T. M. Rice, Phys. Rev. B **37**, 3759 (1988).
[60]A. Moreo and E. Dagotto, Phys. Rev. B **42**, 4786 (1990).
[61]W. Stephan and P. Horch, Phys. Rev. Lett. **66**, 2258 (1991).
[62]J. Zaanen and A. M. Olés, Phys. Rev. B **37**, 9423 (1988).
[63]H. Fukuyama, H. Matsukawa, and Y. Hasegawa, J. Phys. Soc. Jpn. **58**, 364 (1989).
[64]S. Ishihara, H. Matsumoto, and M. Tachiki, Phys. Rev. B **42**, 10 041 (1990).
[65]Q. Si, J. H. Kim, J. P. Lu, and K. Levin, Phys. Rev. B **42**, 1033 (1990).
[66]A. Virosztek and J. Ruvalds, Phys. Rev. B **42**, 4064 (1990).
[67]H. Kohno and K. Yamada, Prog. Theor. Phys. **85**, 13 (1991).
[68]P. W. Anderson, Science **235**, 1196 (1987); P. W. Anderson, G. Baskaran, Z. Zou, and T. Hsu, Phys. Rev. Lett. **58**, 2790 (1987).
[69]R. B. Laughlin, Phys. Rev. Lett. **60**, 2677 (1988).
[70]X. G. Wen, F. Wilczek, and A. Zee, Phys. Rev. B **39**, 11 413 (1989).
[71]N. Nagaosa and P. A. Lee, Phys. Rev. Lett. **62**, 1564 (1989).
[72]C. M. Varma, P. B. Littlewood, S. Schmitt-Rink, E. Abrahams, and A. Ruckenstein, Phys. Rev. Lett. **63**, 1996 (1989).
[73]H. Matsumoto, M. Sasaki, S. Ishihara, and M. Tachiki, preceding paper, Phys. Rev. B **46**, 3009 (1992).
[74]Tohyama and S. Maekawa, J. Phys. Soc. Jpn. **60**, 53 (1991).
[75]J. Wagner, W. Hanke, and D. J. Scalapino, Phys. Rev. B **43**, 10 517 (1991).
[76]H. Eskes, M. B. J. Meinders, and G. A. Sawatzky, Phys. Rev. Lett. **67**, 1035 (1991).
[77]J. Hubbard, Proc. R. Soc. London, Ser. A **276**, 238 (1963); **277**, 237 (1963); **281**, 401 (1964).